

# Monte Carlo Simulations of the Photospheric Process

Rodolfo Santana,<sup>1\*</sup> Patrick Crumley,<sup>1,2,3</sup> Roberto A. Hernández,<sup>1,2</sup> & Pawan Kumar<sup>1</sup>

<sup>1</sup>*Department of Astronomy, University of Texas at Austin, Austin, TX, 78712, USA*

<sup>2</sup>*Department of Physics, University of Texas at Austin, Austin, TX, 78712, USA*

<sup>3</sup>*Astronomical Institute Anton Pannekoek, University of Amsterdam, P.O. Box 94249, 1090 GE Amsterdam, the Netherlands*

Accepted XXX. Received YYY; in original form ZZZ

## ABSTRACT

We present a Monte Carlo (MC) code we wrote to simulate the photospheric process and to study the photospheric spectrum above the peak energy. Our simulations were performed with a photon to electron ratio  $N_\gamma/N_e = 10^5$ , as determined by observations of the GRB prompt emission. We searched an exhaustive parameter space to determine if the photospheric process can match the observed high-energy spectrum of the prompt emission. If we do not consider electron re-heating, we determined that the best conditions to produce the observed high-energy spectrum are low photon temperatures and high optical depths. However, for these simulations, the spectrum peaks at an energy below 300 keV by a factor  $\sim 10$ . For the cases we consider with higher photon temperatures and lower optical depths, we demonstrate that additional energy in the electrons is required to produce a power-law spectrum above the peak-energy. By considering electron re-heating near the photosphere, the spectrum for these simulations have a peak-energy  $\sim 300$  keV and a power-law spectrum extending to at least 10 MeV with a spectral index consistent with the prompt emission observations. We also performed simulations for different values of  $N_\gamma/N_e$  and determined that the simulation results are very sensitive to  $N_\gamma/N_e$ . Lastly, in addition to Comptonizing a Blackbody spectrum, we also simulate the Comptonization of a  $f_\nu \propto \nu^{-1/2}$  fast cooled synchrotron spectrum. The spectrum for these simulations peaks at  $\sim 10^4$  keV, with a flat spectrum  $f_\nu \propto \nu^0$  below the peak energy.

**Key words:** gamma-rays bursts: theory – methods: numerical–radiation mechanisms: non-thermal

## 1 INTRODUCTION

One of the major open questions in the GRB field is, what is the radiation mechanism that produces the observed gamma-ray spectrum, i.e. the Band function (Band et al. 1993)? The Band function is a non-thermal broken power-law spectrum with the peak-energy typically observed at  $\sim 300$  keV (Kaneko et al. 2006). Below (above) the peak-energy, the observed spectrum is a single power-law with a typical spectrum  $f_\nu \propto \nu^{-1.2}$  ( $f_\nu \propto \nu^0$ ) in the energy range  $\sim 300$  keV–10 MeV ( $\sim 10$  keV–300 keV) (Preece et al. 2000). In order to explain the prompt emission, a radiation mechanism must be able to explain all these in the observed spectrum.

The three main mechanisms that have been studied to try and reproduce the Band spectrum are synchrotron, synchrotron self-Compton (SSC), and the photospheric process (See Piran 2004; Zhang 2014; Kumar & Zhang 2015, for reviews on the GRB radiation mechanism). In this work, we focus on the photospheric process (Goodman 1986;

Paczynski 1990; Thompson 1994; Ghisellini & Celotti 1999; Mészáros & Rees 2000; Mészáros et al. 2002; Rees & Mészáros 2005; Thompson et al. 2007), which involves photons undergoing multiple scatterings with hot electrons below the photosphere (Comptonization). Although not a necessary condition for the Comptonization of photons, studies on the photospheric process typically consider the photons to initially have a Blackbody (BB) spectrum, with the peak of the BB spectrum taken to match the observed peak energy of the prompt emission. With an initial seed BB spectrum, the goal of the photospheric process is to broaden the BB spectrum so that it matches the observed Band function. In this work, we focus on models of the photospheric process where the broadening is due to hot electrons scattering photons to higher energies multiple times, where a baryon dominated jet (Pe’er et al. 2006; Lazzati & Begelman 2010; Toma et al. 2011; Lazzati et al. 2013; Chhotray & Lazzati 2015), a Poynting dominated jet (Giannios 2008; Bégué & Pe’er 2015), and a hybrid jet system with both baryons and magnetic fields (Gao & Zhang 2015) have all been considered. Models of the photospheric

\* E-mail: santana@astro.as.utexas.edu (RS)

process where the broadening is due to geometrical effects have also been investigated (Pe'er 2008; Pe'er & Ryde 2011; Mizuta et al. 2011; Ruffini et al. 2013; Bégué et al. 2013; Lundman et al. 2013; Ito et al. 2014; Bégué & Iyyani 2014). See Vereshchagin 2014 and Pe'er 2015 for reviews on the photospheric process.

The basic picture of the photospheric process is as follows. The photons are assumed to be produced below the photosphere. At an optical depth  $\tau \sim \text{few} - 100$ , a dissipation event is assumed to occur, which accelerates the electrons to mildly relativistic or relativistic speeds<sup>1</sup>. In the photospheric process, the average energy of the photons is taken to be much smaller than the average energy of the electrons. Thus, while the outflow is still optically thick, the photons and electrons undergo multiple scatterings, and a photon gains energy from the electrons until its energy reaches the average electron energy or until it escapes the photosphere. The Comptonization of BB photons by hot electrons is predicted to produce a power-law spectrum above the BB peak because only a fraction  $f$  of the photons get scattered once by a hot electron to higher energies, only a fraction  $f^2$  of the photons get scattered twice by a hot electron to higher energies, and so on (Lazzati & Begelman 2010; Ghisellini 2013). Once the outflow reaches the photospheric radius, the medium becomes optically thin and the photons escape the outflow. The resulting observed spectrum is, a peak determined by the BB temperature of photons, and it has a power-law above the peak energy<sup>2</sup>.

An important quantity needed to simulate the photospheric process is the ratio of photons to electrons, which we now estimate for the prompt emission. The kinetic energy of the GRB jet is  $E_{KE} = N_p m_p c^2 \Gamma$ , where  $N_p$  is the number of protons. We consider the kinetic energy of the jet to be carried primarily by protons. Then, taking most of the photons during the prompt emission to have an energy near the peak energy of the spectrum ( $E_{pk}$ ), the energy radiated in gamma-rays is  $E_\gamma = N_\gamma E_{pk}$ . With these two expressions, we can calculate the ratio of  $E_\gamma$  to  $E_{KE}$ :

$$\frac{E_\gamma}{E_{KE}} = \frac{N_\gamma E_{pk}}{N_p m_p c^2 \Gamma}. \quad (1)$$

Taking  $N_p = N_e$  (if few electron-positron pairs are created in the GRB jet, then  $N_p \approx N_e$  due to charge neutrality) and defining the efficiency in the conversion of kinetic energy of the jet to prompt radiation as  $\eta = E_\gamma / (E_\gamma + E_{KE})$ , we can solve for the photon to electron ratio  $N_\gamma / N_e$  (Chhotray & Lazzati 2015)

$$\frac{N_\gamma}{N_e} = 10^6 \left( \frac{\eta}{1 - \eta} \right) \left( \frac{\Gamma}{300} \right) \left( \frac{E_{pk}}{300 \text{ keV}} \right)^{-1}. \quad (2)$$

<sup>1</sup> The dissipation events discussed in the literature for the photospheric process are magnetic reconnection (Thompson 1994; Giannios & Spruit 2005; Giannios 2006, 2012) and internal shocks (Daigne & Mochkovitch 2002; Lazzati & Begelman 2010; Toma et al. 2011; Lazzati et al. 2013).

<sup>2</sup> One of the major difficulties of the photospheric process is reproducing the typically observed low-energy spectrum  $f_\nu \propto \nu^0$ . In this work, we ignore the low-energy spectrum issue and focus on the high-energy spectrum. For detailed discussions on the low-energy index of the photospheric process, see Vurm et al. 2013; Lundman et al. 2013; Deng & Zhang 2014.

In this expression, we have normalized  $\Gamma$  and  $E_{pk}$  to typical values. Taking an efficiency  $\eta \sim 10\%$ , the photon to electron ratio is  $N_\gamma / N_e \sim 10^5$ . Thus, a ratio of photons to electrons  $\sim 10^5$  is required to simulate the photospheric process (Lazzati & Begelman 2010; Chhotray & Lazzati 2015).

Previous MC photospheric works have demonstrated that there is a power-law above the peak of the spectrum for  $N_\gamma / N_e \sim 10^1 - 10^4$ , where  $N_\gamma$  ( $N_e$ ) is the number of photons (electrons) considered (Lazzati & Begelman 2010; Chhotray & Lazzati 2015). However, whether the power-law above the peak of the spectrum is a robust feature of the photospheric process is still in question since realistic simulations with  $N_\gamma / N_e = 10^5$  have not been performed. We developed a new MC photospheric code capable of performing simulations for realistic GRB  $N_\gamma / N_e$  ratios. In this work, we present results for MC photospheric simulations with  $N_\gamma / N_e = 10^5$  for the first time. We also perform an exhaustive parameter space search to determine if the photospheric process can produce the observed high-energy spectral index of the Band function. In addition, we include adiabatic cooling of photons and electrons, which was neglected by previous MC photospheric codes (Lazzati & Begelman 2010; Chhotray & Lazzati 2015).

Another possible source for the seed photons is the synchrotron process. Therefore, in addition to considering the Comptonization of a BB spectrum of photons, we also consider the Comptonization of a seed photon spectrum  $f_\nu \propto \nu^{-1/2}$ , the expected synchrotron spectrum when electrons are in the fast cooling regime (Sari et al. 1996; Ghisellini et al. 2000). We use our MC photospheric code to study how Comptonization modifies this seed spectrum.

This work is organized as follows. In Section 2, we describe the algorithm of our MC photospheric code (the expressions for the implementation can be found in the Appendices). In Section 3, we discuss the parameters we explore for our MC photospheric simulations with a seed BB spectrum. The simulation results for the Comptonization of a seed BB spectrum are discussed in Section 4 and the interpretation of these results is discussed in Section 5. In Section 6, we discuss the parameters we explore for our simulations on the Comptonization of a seed  $f_\nu \propto \nu^{-1/2}$  spectrum, the results for these simulations, and the interpretation of these results. Lastly, in Section 7, we discuss our conclusions.

## 2 DESCRIPTION OF MONTE CARLO PHOTOSPHERIC CODE

In this section, we give an overview of our MC photospheric code algorithm. The details for implementation can be found in the Appendices. Our code was written in the C++11 programming language and we used the GCC version 4.9.2 compiler. Under 9 GB of RAM are needed for a simulation with  $10^8$  photons and a simulation initialized at  $\tau_{\text{initial}} = 2$  takes under 2 hours in a regular desktop Linux machine (see definition of  $\tau_{\text{initial}}$  below). Lastly, we note that our code is not parallelized; each scattering event between a photon and an electron is performed one by one.

## 2.1 Input Parameters for Simulations with Seed BB Photons

The input parameters for our MC photospheric simulations with a seed BB spectrum of photons are described below. In Section 6, we will discuss the input parameters for the simulations with a  $f_\nu \propto \nu^{-1/2}$  seed spectrum. In the discussion below and throughout this work, unprimed (primed) quantities refer to quantities in the observer (jet-comoving) frame.

- $\Gamma$  — The bulk Lorentz factor of the outflow. We consider a typical  $\Gamma = 300$  for GRBs (Molinari et al. 2007; Xue et al. 2009; Liang et al. 2010).

- $L$  — The isotropic equivalent kinetic luminosity of the outflow. We consider  $L = 10^{52}$  ergs/sec (Liang et al. 2007; Wanderman & Piran 2010).

- $N_e$  — The number of electrons in a simulation. We consider  $N_e = 10^3$ , the same number of electrons as previous MC photospheric simulations (Lazzati & Begelman 2010; Chhotray & Lazzati 2015). In Section 2.5, we explicitly show that  $10^3$  electrons are enough to get an accurate representation for an electron distribution.

- Electron Distribution — We consider three different distributions for the electrons: 1. mono-energetic electrons (all electrons initialized to the same electron Lorentz factor  $\gamma'_e$ ), with the initial  $\gamma'_e$  of the electrons as the input parameter. 2. Maxwell-Boltzmann (MB) distribution of electrons with the electron temperature  $T'_e$  as an input parameter. 3. Power-Law distribution of electrons  $dN_e/d\gamma'_e \propto (\gamma'_e)^{-p}$  ranging from  $\gamma'_{e,1}$  to  $\gamma'_{e,2}$ , with the electron Lorentz factors  $\gamma'_{e,1}$ ,  $\gamma'_{e,2}$ , and the electron index  $p$  as input parameters.

- $\tau_{\text{initial}}$  — The optical depth corresponding to the distance from the central engine where the photons are initialized (see Equation 3). We consider  $\tau_{\text{initial}} = 2, 8, 16$ .

- $N_\gamma$  — The number of photons in a simulation. Since we typically consider  $N_e = 10^3$ , to reach  $N_\gamma/N_e = 10^5$ , we consider  $N_\gamma = 10^8$  for our simulations.

- $T'_\gamma$  — The photons are initialized to have a Blackbody (BB) distribution with temperature  $T'_\gamma$ .

- $N_{\text{collect}}$  — The number of photons collected for the output spectrum. We consider  $N_{\text{collect}} = N_\gamma/3$  for our simulations as in Lazzati & Begelman 2010 since considering  $N_{\text{collect}} = N_\gamma/3$  allows for enough scatterings to occur so that the electrons can cool by IC scatterings. By plotting the first  $N_\gamma/3$  photons that escape the photosphere for an output spectrum, we are plotting a time-averaged spectrum.

## 2.2 Initializing Electrons and Photons

The first step of our MC photospheric simulations is to initialize the electrons and photons. The only property we track in the observer frame is the position of the photons to determine if they have escaped the photosphere. All the other properties and calculations are done in the jet-comoving frame.

### 2.2.1 Initialization of Direction and Energy of Electrons

The directions of the momentum of the  $N_e$  electrons are drawn randomly in the jet-comoving frame (see Appendix B1 for algorithm). The  $\gamma'_e$  for each of the  $N_e$  electrons is

drawn from the distribution specified in the input parameters (see Appendix B2 for algorithm). We assume that the electrons are distributed uniformly in the jet and do not track their position.

### 2.2.2 Initialization of Direction, Energy, and Position of Photons

The directions of the momentum of the  $N_\gamma$  photons are drawn randomly in the jet-comoving frame (see Appendix C1 for algorithm). The energy of each of the  $N_\gamma$  photons in the jet-comoving frame ( $E'_\gamma$ ) is drawn from either a BB distribution with temperature  $T'_\gamma$  or a power-law distribution (depending on the system being investigated) (see Appendix C2 for algorithm).

The origin of the coordinate system we use to track the position of the photons in the observer frame is the central engine. The  $N_\gamma$  photons are initially placed randomly and uniformly within an angle  $\leq 1/\Gamma$  (jet opening angle) in the direction of the observer at a distance

$$R_{\text{initial}} = \frac{L\sigma_T}{8\pi m_p c^3 \beta \Gamma^3 \tau_{\text{initial}}}, \quad (3)$$

where  $\sigma_T$  is the Thomson cross section and  $\beta = \sqrt{1 - \Gamma^{-2}}$  is the speed of the outflow divided by the speed of light.

We then draw the distance  $s'$  each photon travels in the jet-comoving frame before running into an electron randomly from the probability density  $p(s') \propto \exp(-s'/\ell'_{\text{mfp}})$ , where  $\ell'_{\text{mfp}}$  is the mean free path. Inverting this probability density,  $s'$  is sampled with the formula  $s' = -\ell'_{\text{mfp}} \ln(\xi)$ , where  $\xi$  is a uniformly distributed random number between 0 and 1. The mean free path and the electron density ( $n'_e$ ) are given by

$$\ell'_{\text{mfp}}(R) = \frac{1}{n'_e(R)\sigma_T} \quad (4)$$

$$n'_e(R) = \frac{L}{4\pi R^2 m_p c^3 \Gamma^2}, \quad (5)$$

where  $R$  is the distance of the photon from the central engine in the observer frame. The distance each photon travels in the jet comoving frame is then Lorentz transformed to the observer frame to determine the new location of the photon in the observer frame (see Appendix C3 for algorithm).

## 2.3 Adiabatic Cooling of Photons and Electrons

As the jet expands outward, the energy of the photons and electrons decreases due to adiabatic cooling. Adiabatic cooling depends on the radial distance traveled by the jet, with the energy of the photons decreasing by a factor  $r^{-2/3}$  and the kinetic energy of the electrons decreasing by a factor  $r^{-2/3}$  or  $r^{-4/3}$ , depending on whether an electron is relativistic or sub-relativistic. This scaling is valid as long as the radial width of the jet does not change with distance, which is satisfied for highly relativistic jets below the photosphere. Thus, in between scattering events, the expressions we use to update the energy of a photon and the  $\gamma'_e$  of an electron

due to adiabatic cooling are

$$\frac{E'_{\gamma,f}}{E'_{\gamma,i}} = \left( \frac{R_{\text{initial}} + (t_\gamma + \Delta t_\gamma)\beta_j c}{R_{\text{initial}} + t_\gamma\beta_j c} \right)^{-2/3} \quad (6)$$

$$\frac{\gamma'_{e,f} - 1}{\gamma'_{e,i} - 1} = \left( \frac{R_{\text{initial}} + (t_\gamma + \Delta t_\gamma)\beta_j c}{R_{\text{initial}} + t_e\beta_j c} \right)^{2-2(4\gamma'_{e,i}+1)/(3\gamma'_{e,i})}. \quad (7)$$

In these equations,  $R_{\text{initial}}$  corresponds to the distance where the photons are initialized (Equation 3) and the subscript  $i$  ( $f$ ) corresponds to a photon and electron property before (after) the photon travels a distance  $s'$  (in the jet comoving frame).  $t_\gamma$  ( $t_e$ ) represents the total time elapsed for a photon (electron) in between scattering events (in the observer frame). Thus, in the time  $t_\gamma$  ( $t_e$ ), the jet has traveled a radial distance  $t_\gamma\beta_j c$  ( $t_e\beta_j c$ ) and the radial position of the photon (electron) before the photon travels a distance  $s'$  is  $R_{\text{initial}} + t_\gamma\beta_j c$  ( $R_{\text{initial}} + t_e\beta_j c$ ).  $\Delta t_\gamma$  represents the time it takes a photon to travel a distance  $s'$  (in the observer frame, see Appendix C3); thus, the final radial position of the photon and electron are  $R_{\text{initial}} + (t_\gamma + \Delta t_\gamma)\beta_j c$ . Lastly, we note that the  $(4\gamma'_{e,i} + 1)/(3\gamma'_{e,i})$  term in the exponent of Equation 7 is used to take into account that the electron adiabatic index transitions from 4/3 to 5/3 as the electron cools due to IC scatterings and adiabatic expansion.

## 2.4 Main MC Photospheric Program

The first step in our main program is to check for photons that were able to escape the photosphere, without interacting with an electron, with the first  $s'$  drawn.  $R_{\text{photosphere}}$  is defined as the radius where  $\tau = 1$  in Equation 3. If a photon was able to escape the photosphere, we Doppler boost its energy to the observer frame with the Doppler factor,  $\mathcal{D}E'_\gamma$ , and store this energy. Otherwise, we place this photon in a priority queue data structure. Each element in the priority queue is a tuple with entries  $(t_{\gamma,k}, k)$ , where  $k$  refers to the index of a photon in an array and  $t_{\gamma,k}$  refers to the total elapsed time in between scatterings of this particular photon (in the observed frame). With the photons in a priority queue, the photon with the smallest  $t_{\gamma,k}$  gets scattered first (is given priority) and then the photon with the next smallest  $t_{\gamma,k}$  gets scattered next and so on (Lazzati & Begelman 2010). Having the array index of the photon ( $k$ ) allows us to access the properties of this particular photon (energy, direction, and position).

In the next part of the program, we take into account adiabatic cooling and determine whether a photon-electron scattering event will occur. We first draw one of the  $N_e$  electrons randomly. Then, we use the  $s'$  of the first photon in the priority queue (photon with smallest  $t_{\gamma,k}$ ) to propagate this photon forward (see Appendix C3 for algorithm). After using Equations 6 - 7 to take into account adiabatic cooling, we calculate the dimensionless photon energy of this particular photon in the rest frame of this particular electron (defined as  $x'_i$ ) and the cross-section for this interaction (defined as  $\sigma(x'_i)$ ; see Appendix D for algorithm). The probability that the scattering event will occur is  $\sigma(x'_i)/\sigma_T$ , where  $\sigma(x'_i) \leq \sigma_T$ . To determine if the scattering event occurs, we draw a uniformly distributed random number between 0 and 1, defined as  $\xi_s$ . If  $\xi_s \leq \sigma(x'_i)/\sigma_T$ , the scattering event occurs. If the scattering event occurs, we update the energy and direction of the photon (see Appendix D for algorithm) and

the energy and direction of the electron (see Appendix E for details) after the scattering event. Then (regardless of whether the scattering event occurred or not), we draw a new  $s'$  at the current location  $R$  of the photon with the expression  $s'(R) = -\ell'_{\text{mfp}}(R)\ln(\xi)$ . The distance the photon travels in the jet-comoving frame is then Lorentz transformed to the observer frame to check if the photon has escaped the photosphere. If  $R \geq R_{\text{photosphere}}$  is satisfied, we store the energy of this photon in the observer frame ( $\mathcal{D}E'_\gamma$ ). Otherwise, we place this photon back in the priority queue with the new  $t_{\gamma,k}$ . We repeat the process described in this paragraph until  $N_{\text{collect}}$  photons have escaped the photosphere.

## 2.5 MC Photospheric Code Tests

To test our code, we compared our simulation results to the MC photospheric code results from Lazzati & Begelman (2010). In the left panel of Figure 1, we compare our simulation results to the three simulations in Figure 4 of Lazzati & Begelman (2010). In this figure and throughout this work,  $f_\nu$  represents the specific flux, the flux per unit frequency  $\nu$ , in the observer frame. For these simulations, we use the same input parameters as Lazzati & Begelman (2010):  $\Gamma = 1000$ ,  $k_B T'_\gamma = 90$  eV,  $N_\gamma = 3 \times 10^6$ ,  $N_e = 10^3$ ,  $N_{\text{collect}} = N_\gamma/3$ , mono-energetic electrons initialized to  $\gamma'_e = 2$ ,  $\tau_{\text{initial}} = 2, 8, 16$ , and no adiabatic cooling. There is good agreement for all the simulations. To quantify this agreement, we performed Kolmogorov-Smirnov (KS) tests. The probability that our simulations are drawn from the same distribution as those of Lazzati & Begelman (2010) (P-values) are 0.9999 for  $\tau_{\text{initial}} = 2$ , 0.9862 for  $\tau_{\text{initial}} = 8$ , and 0.9809 for  $\tau_{\text{initial}} = 16$ . This good agreement demonstrates that our MC photospheric code is working properly.

We next perform a test to determine if  $10^3$  electrons are enough to represent an electron distribution. If there are not enough electrons, the photon spectrum will look very noisy. Previous MC photospheric studies (Lazzati & Begelman 2010; Chhotray & Lazzati 2015) found that  $10^3$  electrons are enough to represent an electron distribution; however, their simulations were performed for lower  $N_\gamma/N_e$ . To determine if  $10^3$  electrons are enough for our  $N_\gamma/N_e = 10^5$  simulations, we perform 2 simulations with  $N_\gamma = 10^9$ ,  $N_e = 10^4$  (10 times more photons and electrons) and compared them to simulation results with  $N_\gamma = 10^8$ ,  $N_e = 10^3$  in right panel of Figure 1 (we used the input parameters described in Section 2.1 for mono-energetic electrons with initial  $\gamma'_e = 2$ ,  $30 k_B T'_\gamma = 300$  eV,  $\Gamma = 300$ , and adiabatic cooling). From KS tests, the probability that the two  $\gamma'_e = 2$  [ $\gamma'_e = 30$ ] simulations are drawn from the same distribution is 0.9999 [0.9999]. This good agreement explicitly demonstrates that  $10^3$  electrons are enough for  $N_\gamma/N_e = 10^5$  simulations.

## 3 PARAMETERS CONSIDERED FOR MC SIMULATIONS WITH SEED BB PHOTONS

We now discuss the range of parameters we consider for our simulations. The main input parameters that affect the output spectrum are  $k_B T'_\gamma$  (determines the energy of the majority of the photons),  $\gamma'_e$  (determines energy in the electrons), and  $\tau_{\text{initial}}$  (determines the average number of scatterings before a photon arrives at the photosphere).  $L$  determines the

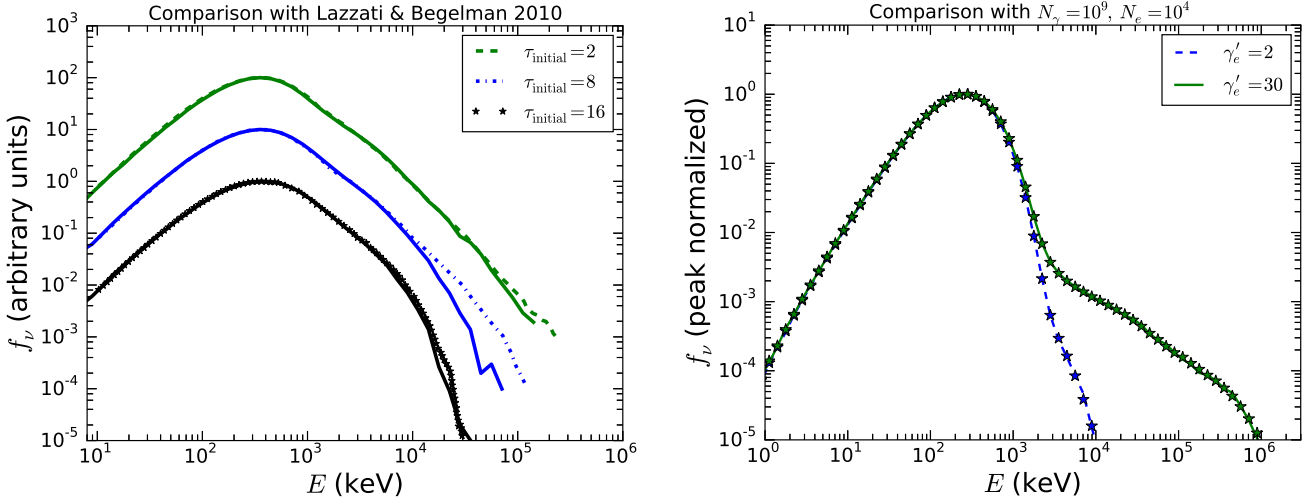


**Figure 1.** *Left Panel:* Comparison of our MC photospheric simulation results (solid lines) to those from Figure 4 of Lazzati & Begelman (2010) (dotted lines, dash dotted lines, and stars). These simulations are for the Comptonization of seed BB photons with  $k_B T'_\gamma = 90$  eV,  $\Gamma = 1000$  with mono-energetic electrons with initial  $\gamma'_e = 2$ ,  $\tau_{\text{initial}} = 2, 8, 16$ , and no adiabatic cooling. *Right Panel:* Comparison of  $N_\gamma = 10^9, N_e = 10^4$  (stars) simulation results to  $N_\gamma = 10^8, N_e = 10^3$  (dotted and solid lines) simulation results. The simulations are for the Comptonization of seed BB photons with  $k_B T'_\gamma = 300$  eV,  $\Gamma = 300$  with mono-energetic electrons with initial  $\gamma'_e = 2, 30$ ,  $\tau_{\text{initial}} = 2$ , and adiabatic cooling.

physical scales of the system by determining  $R_{\text{initial}}, R_{\text{photosphere}}, n'_e$ , and  $\ell'_{\text{mfp}}$ , but it does not affect the number of scatterings or the shape of the spectrum. The main effect of  $\Gamma$  is to Doppler boost the photon spectrum to the observer frame. In addition,  $\Gamma$  also determines the physical scales of the system by determining  $R_{\text{initial}}, R_{\text{photosphere}}, n'_e$ , and  $\ell'_{\text{mfp}}$ .

For our simulations, we considered  $k_B T'_\gamma = 30$  eV, 100 eV, 300 eV. One way the photon temperature can affect the output spectrum is through the production of electron-positron pairs by photon annihilation, which would decrease (increase) the number of photons (electrons) in a simulation. However, since the typical photon energies we are considering  $k_B T'_\gamma \sim 30$  eV – 300 eV are much less than  $m_e c^2$ , electron-positron pair production is expected to be unimportant and we neglect it for our simulations. Another more important effect  $k_B T'_\gamma$  has on the simulation results is on the cooling of electrons. The photons in the jet-comoving frame are more energetic for larger  $k_B T'_\gamma$  and more energetic photons will cool the electrons faster when they undergo multiple scatterings.

$\gamma'_e$  is an important parameter since it determines the available energy electrons have to transfer to photons. The smallest value we consider for  $\gamma'_e$  is 2. In the photospheric process, in order to avoid synchrotron cooling from the magnetic field that is expected to be present in the jet, the synchrotron emission is taken to be self-absorbed. The largest  $\gamma'_e$  that can be considered is found by setting the optical depth for synchrotron self-absorption equal to 1. Below, we calculate the largest  $\gamma'_e$  allowed for MB and PL distributions of electrons.

For a MB distribution distribution of electrons, the synchrotron self-absorption optical depth  $\tau_{\text{syn}}^{\text{MB}}$  is given by (Rybicki & Lightman 1979; Lazzati & Begelman 2010)

$$\tau_{\text{syn}}^{\text{MB}} = \frac{10^6}{(\gamma'_e)^5 \epsilon_B^{1/2} (E'_\gamma / 1\text{keV})^2}. \quad (8)$$

In this equation,  $\epsilon_B = U_B / U_{\text{rad}}$ , where  $U_B$  ( $U_{\text{rad}}$ ) is the en-

ergy density in the magnetic field (radiation) and we note that  $\tau_{\text{syn}}^{\text{MB}}$  depends on the energy of the photons in the co-moving frame. Setting  $\tau_{\text{syn}}^{\text{MB}} = 1$ , for  $\epsilon_B \sim 0.1$  (magnetic field subdominant to radiation) and  $E'_\gamma \sim 300$  eV ( $E'_\gamma \sim 100$  eV) [ $E'_\gamma \sim 30$  eV], the upper limit we find is  $\gamma'_e \sim 30$  ( $\gamma'_e \sim 50$ ) [ $\gamma'_e \sim 80$ ].

For a power-law distribution distribution of electrons, the synchrotron self-absorption optical depth  $\tau_{\text{syn}}^{\text{PL}}$  is given by (Wu et al. 2003; Gou et al. 2007)

$$\tau_{\text{syn}}^{\text{PL}} = \frac{e}{B'} \left( \frac{(p-1)(p+2)}{(\gamma'_1)^{-(p-1)} - (\gamma'_2)^{-(p-1)}} \right) \times \frac{2\sqrt{6}\pi^{3/2}}{9} (\gamma'_2)^{-(p+4)} \exp(-1) \sigma_T^{-1}. \quad (9)$$

In this equation,  $\gamma'_1$  ( $\gamma'_2$ ) is the electron Lorentz factor where the power-law begins (ends) and  $B'$  is the magnetic field in the jet-comoving frame. From the expressions  $U_B = (B')^2 / (8\pi)$  and  $U_{\text{rad}} = a_{\text{rad}} (T'_\gamma)^4$ ,  $B' = (8\pi \epsilon_B a_{\text{rad}})^{1/2} (T'_\gamma)^2$ . Setting  $\tau_{\text{syn}}^{\text{PL}} = 1$ , taking  $\gamma'_1 = 2$ ,  $p = 2.4$ , and  $B'$  corresponding to  $\epsilon_B = 0.1$  and  $k_B T'_\gamma = 300$  eV ( $k_B T'_\gamma = 100$  eV) [ $k_B T'_\gamma = 30$  eV], the upper limit we found for  $\gamma'_2$  is  $\gamma'_2 \sim 30$  ( $\gamma'_2 \sim 50$ ) [ $\gamma'_2 \sim 80$ ]. Thus, for both a MB distribution and a PL distribution, the maximum  $\gamma'_e$  we can consider for  $k_B T'_\gamma = 300$  eV ( $k_B T'_\gamma = 100$  eV) [ $k_B T'_\gamma = 30$  eV] is  $\sim 30$  ( $\sim 50$ ) [ $\sim 80$ ]. A summary of the values we considered for  $\gamma'_e$  for each value of  $k_B T'_\gamma$  is given in Table 1.

$\tau_{\text{initial}}$  affects the shape of the spectrum since it determines the average number of scatterings a photon experiences before escaping the photosphere. The average number of scatterings for a photon is  $\sim 2\tau_{\text{initial}}$  (Bégué et al. 2013), not  $\sim (\tau_{\text{initial}})^2$ , since as the GRB relativistic outflow moves outward,  $n'_e$  decreases as  $R^2$  (Equation 5). For our simulations, we considered  $\tau_{\text{initial}} = 2, 8, 16$ .

Lastly, since  $N_\gamma \gg N_e$  for our simulations, the electrons rapidly cool by IC scatterings and then the electrons no

$k_B T'_\gamma$	Mono-Energetic	MB	PL Distribution
30 eV	$\gamma'_e = 2, 30, 80$	$\frac{k_B T'_e}{(\gamma_{\text{ad,el}}-1)m_e c^2} = (2-1), (80-1)$	$\gamma'_{e,1} = 2, \gamma'_{e,2} = 80, p = 2.4$
100 eV	$\gamma'_e = 2, 30, 50$	$\frac{k_B T'_e}{(\gamma_{\text{ad,el}}-1)m_e c^2} = (2-1), (50-1)$	$\gamma'_{e,1} = 2, \gamma'_{e,2} = 50, p = 2.4$
300 eV	$\gamma'_e = 2, 10, 30$	$\frac{k_B T'_e}{(\gamma_{\text{ad,el}}-1)m_e c^2} = (2-1), (30-1)$	$\gamma'_{e,1} = 2, \gamma'_{e,2} = 30, p = 2.4$

**Table 1.**  $\gamma'_e$  values we consider for our simulations for each value of  $k_B T'_\gamma$  and the 3 different electron distributions we consider. For the MB distribution, we give the value of  $k_B T'_e = (\gamma_{\text{ad,el}} - 1)(\gamma'_e - 1)m_e c^2$ , where  $\gamma_{\text{ad,el}} = (4\gamma'_e + 1)/(3\gamma'_e)$  is the electron adiabatic index, since  $k_B T'_e$  measures the kinetic energy of the electrons.

longer have much energy to transfer to the photons. Thus, we also considered electron re-heating. At a given  $\tau_{\text{initial}}$ , the total number of scatterings expected is  $\sim 2\tau_{\text{initial}}N_\gamma$ . To re-heat the electrons, we first specify the number of re-heating events  $N_{\text{th}}$  we choose to consider. Then, after  $(2\tau_{\text{initial}}N_\gamma)/(N_{\text{th}} + 1)$  scatterings, we re-heat the electrons to the same distribution that they were initialized to (we divide by  $N_{\text{th}} + 1$  since the total number of heating events is the initial heating event plus  $N_{\text{th}}$  events). We adopt this methodology to have the re-heating events evenly spaced within the total number of scatterings.

In this electron re-heating scheme, since all the electrons are re-accelerated, it corresponds to a global heating mechanism. In GRBs, the heating mechanism is likely to be global, i.e. occurring throughout the causally connected part of the jet, since observations show that the conversion of jet energy to gamma-ray radiation is an efficient process (Granot et al. 2006; Fan & Piran 2006; Zhang et al. 2007). The electrons can be re-accelerated by magnetic reconnection in a Poynting flux dominated jet or by shocks in a baryon dominated jet.

#### 4 SIMULATION RESULTS FOR COMPTONIZATION OF SEED BB SPECTRUM

In this section, we first show our results for one dissipation event, where electrons are only accelerated once at the start of the simulation. Then, we consider electron re-heating, where the electrons are re-accelerated back to their initial distribution  $N_{\text{th}}$  times.

##### 4.1 Simulation Results for One Dissipation Event

In Figure 2, we show simulations for  $\tau_{\text{initial}} = 2$ , the three values we considered for  $k_B T'_\gamma$ , and mono-energetic electrons with the values of  $\gamma'_e$  shown in Table 1. As the reader may have noticed in Figure 1, the most striking feature of the output spectrum is the sharp drop in  $f_\nu$  by  $\sim 2$  orders of magnitude after the peak energy,  $E_{\text{pk}}$ . Unlike previous studies for  $N_\gamma/N_e = 1 - 10^4$ , our results for  $N_\gamma/N_e = 10^5$  do not show a power-law immediately after the peak energy. After the drop in  $f_\nu$ , the simulations with  $\gamma'_e = 2$  in the three panels continue to decline rapidly. On the other hand, the simulations with  $\gamma'_e \sim 10 - 80$  in each panel display a power-law for  $\sim 2 - 3$  decades in energy before declining rapidly again. The highest energy the photons near the BB peak can attain after one scattering is  $\sim 4 \times (100 \text{ eV})\Gamma(\gamma'_e)^2 \sim 10^5 \text{ keV}$  for

$\gamma'_e \sim 50$ . Once the photons reach these energies, IC scattering is highly Klein-Nishina (KN) suppressed, leading to an exponential decay in the spectrum for higher energies.

In Figure 3, we show simulation results for  $\tau_{\text{initial}} = 2$ , the three values we considered for  $k_B T'_\gamma$ , and the largest  $\gamma'_e$  we considered for each distribution in Table 1. In each panel, the PL distribution simulations display the least broadened spectrum. This is due to the fact that the PL distribution contains the least energetic electrons among these three distributions. The mono-energetic and MB electron distribution simulations show similar results since the two distributions are similar; the MB distribution has an average  $\gamma'_e$  very close to the  $\gamma'_e$  value we consider for the mono-energetic electrons. After the sharp drop in  $f_\nu$  in each panel, all the simulations display a single power-law spectrum for  $\sim 3$  decades in energy.

In Figure 4, we show simulation results for  $\tau_{\text{initial}} = 2, 8, 16$ , the three values of  $k_B T'_\gamma$  we considered, and MB electrons with the largest value we considered for  $\gamma'_e$  (see Table 1). In addition, in each panel, we also plot the energy spectrum  $f_\nu = EN_E$  of the kinetic energies of the electrons at the end of each simulation in the observer frame, i.e.  $m_e c^2(\gamma_e - 1)\Gamma$ . Increasing  $\tau_{\text{initial}}$  has two effects on the output spectrum: decreasing the number of photons at higher energies and increasing the broadening of the spectrum. For larger  $\tau_{\text{initial}}$ , the additional scatterings allow for the high-energy photons to transfer energy back to the electrons. The increase in broadening of the spectrum from  $k_B T'_\gamma = 300 \text{ eV}$  (Top-Left Panel) to  $k_B T'_\gamma = 30 \text{ eV}$  (Bottom-Left Panel) is due to a couple of effects: 1. the larger  $\gamma'_e$  considered for  $k_B T'_\gamma = 30 \text{ eV}$  allows for the electrons to transfer more energy to the photons. 2. for  $k_B T'_\gamma = 30 \text{ eV}$ , the photons have lower energy in the jet-comoving frame, and thus, cool the electrons more slowly, allowing for more photons to be upscattered to higher energies. In each panel, the simulations with larger  $\tau_{\text{initial}}$  have a lower peak-energy due to the adiabatic cooling of photons. In the top-left panel, the three simulations show a sharp drop in  $f_\nu$  by  $\sim 2$  orders of magnitude above the peak energy. In the top-right panel, the  $\tau_{\text{initial}} = 8, 16$  almost show a power-law above the peak-energy, but the spectrum still declines rapidly. Fitting a power-law to the  $\tau_{\text{initial}} = 8, 16$  simulations, we find a steep spectrum  $f_\nu \propto \nu^{-2}$ . In the bottom-left panel, the  $\tau_{\text{initial}} = 8, 16$  simulations show a power-law above the peak-energy, with a  $f_\nu \propto \nu^{-1.2}$  spectrum, in agreement with the Band function. However, the peak-energy for these two spectra is  $\sim 30 \text{ keV}$ , 10 times smaller than the typical peak-energy of the prompt emission.

The electron distributions at the end of all the simulations display a Maxwell-Boltzmann distribution. In each

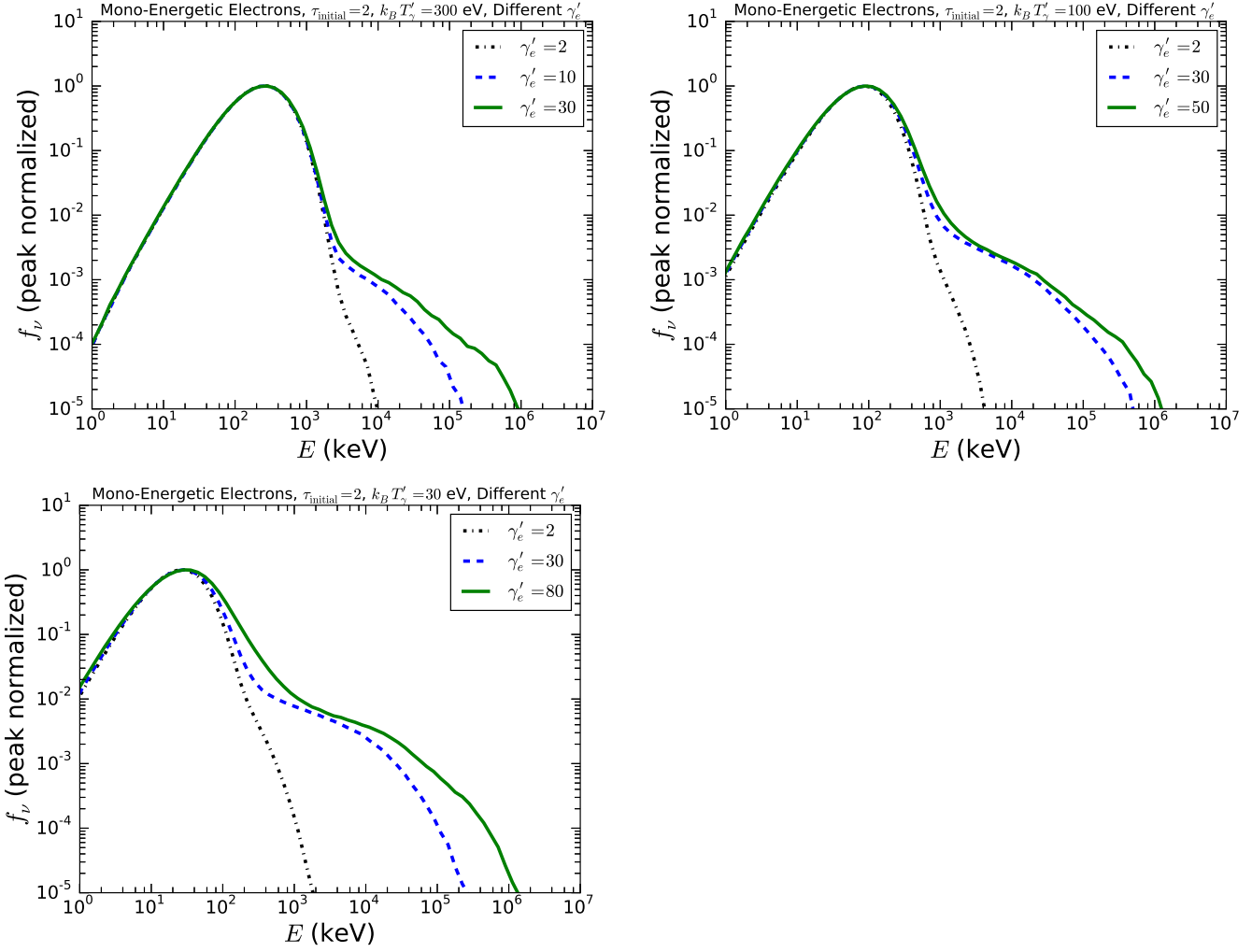


**Figure 2.** *Top-Left panel:* Simulation results for the Comptonization of seed BB photons with  $k_B T'_\gamma = 300$  eV,  $\Gamma = 300$  with mono-energetic electrons with initial  $\gamma'_e = 2, 10, 30$  and  $\tau_{\text{initial}} = 2$ . *Top-Right panel:* Same as *Top-Left panel* for  $k_B T'_\gamma = 100$  eV,  $\Gamma = 300$  and mono energetic electrons with initial  $\gamma'_e = 2, 30, 50$ . *Bottom-Left panel:* Same as *Top-Left panel* for  $k_B T'_\gamma = 30$  eV,  $\Gamma = 300$  and mono energetic electrons with initial  $\gamma'_e = 2, 30, 80$ .

panel, as  $\tau_{\text{initial}}$  increases, the electron distributions become narrower and the electron temperature decreases. This is due to the fact that the additional scatterings allow for the electrons to transfer more energy to the photons.

In summary, we searched a wide parameter space for the photospheric process in Figures 2-4. In Figure 2, for  $\tau_{\text{initial}} = 2$ , there is a sharp drop in  $f_\nu$  above the peak-energy by  $\sim 2$  orders of magnitude for all the photon temperatures and  $\gamma'_e$  values we considered. In Figure 3, we determined that the electron distribution does not have a large impact on the simulation results. In Figure 4, we determined that considering a larger optical depth and a lower photon temperature broadens the BB spectrum more, with a power-law spectrum being developed above the peak-energy for the lowest photon temperature we considered ( $k_B T'_\gamma = 30$  eV). However, the peak-energy for the  $k_B T'_\gamma = 30$  eV and  $\tau_{\text{initial}} = 8, 16$  simulations is a factor of 10 smaller than the typical peak-energy of the prompt emission. In the next subsection, we consider electron re-heating to determine the additional energy that needs to be added to the electrons of the  $k_B T'_\gamma = 100$  eV,

300 eV simulations to produce a power-law above the peak-energy.

#### 4.2 Simulation Results with Electron Re-heating

In the top-left panel of Figure 5, we show electron re-heating results for  $\tau_{\text{initial}} = 5$ ,  $k_B T'_\gamma = 300$  eV, mildly relativistic electrons with initial  $\gamma'_e \sim 2$ , and  $N_{\text{th}} = 10, 100, 1000$ . We considered a larger  $\tau_{\text{initial}}$  (5 as opposed to 2) to allow a larger space for the re-heating events to occur. For  $N_{\text{th}} = 10$ ,  $f_\nu$  still drops after the peak energy by  $\sim 2$  orders of magnitude. For  $N_{\text{th}} = 100$ ,  $f_\nu$  displays a power-law above the peak energy for  $\sim 2$  decades, with a spectrum  $f_\nu \propto \nu^{-1.43}$ . For  $N_{\text{th}} = 1000$ ,  $f_\nu$  also displays a power-law above the peak energy for  $\sim 2$  decades, with a shallower spectrum  $f_\nu \propto \nu^{-0.67}$ . In the top-right panel, we show simulation results for  $\tau_{\text{initial}} = 5$ ,  $k_B T'_\gamma = 300$  eV,  $\gamma'_e \sim 30$ , and  $N_{\text{th}} = 2, 20, 200$ . For  $N_{\text{th}} = 20, 200$ , there is a power-law spectrum above the peak energy for  $\sim 2$  decades, with  $f_\nu \propto \nu^{-1.06}$  for  $N_{\text{th}} = 20$  and  $f_\nu \propto \nu^{-0.34}$  for  $N_{\text{th}} = 200$ . In the bottom-left panel, we show electron re-heating simula-

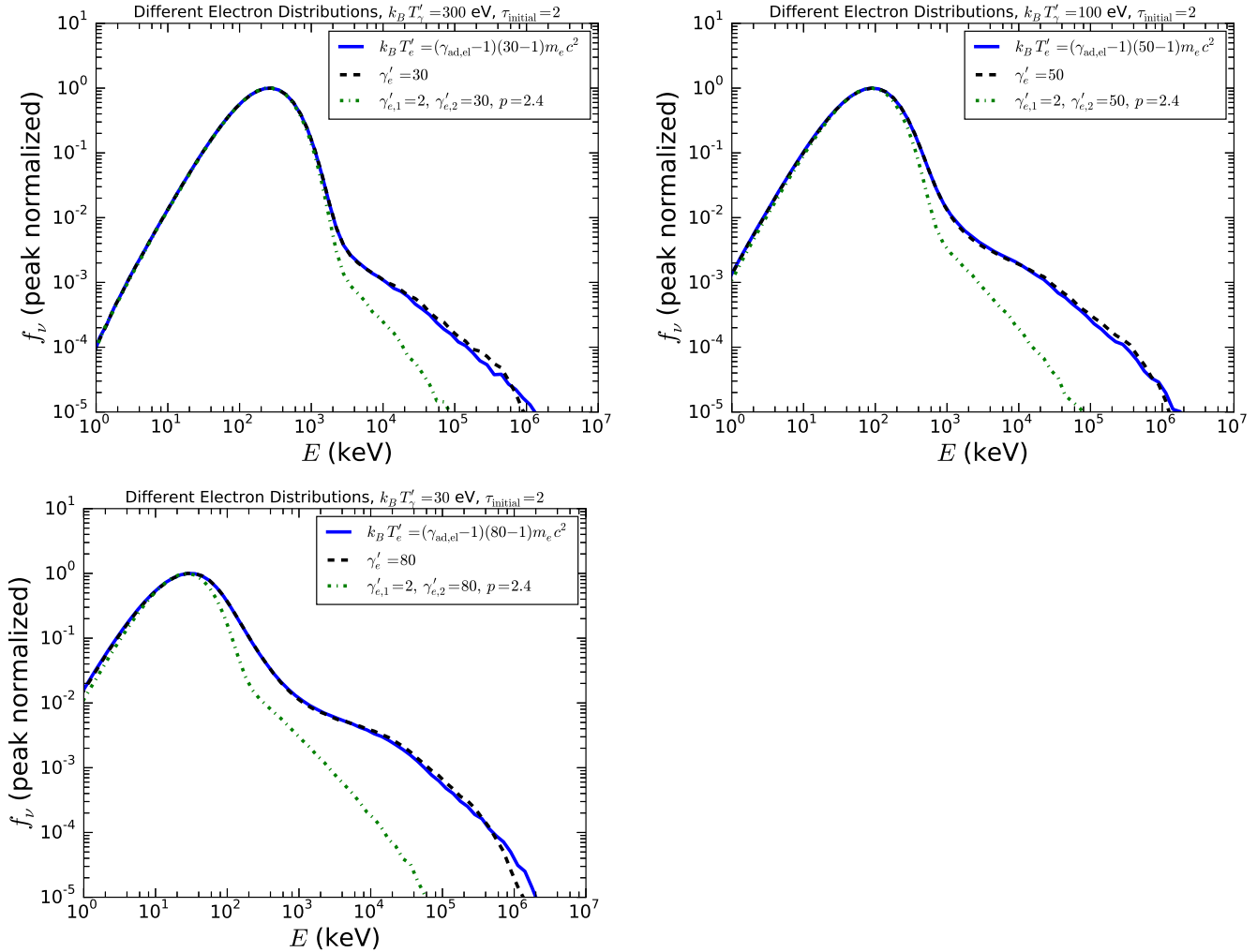


**Figure 3.** *Top-Left panel:* Simulation results for the Comptonization of seed BB photons with  $k_B T'_\gamma = 300$  eV,  $\Gamma = 300$  with electrons following MB, mono energetic, and PL distributions, and  $\tau_{\text{initial}} = 2$ . For each distribution, we considered the largest value of  $\gamma'_e$  we can consider for  $k_B T'_\gamma = 300$  eV (see discussion in Section 3 and Table 1). *Top-Right panel:* Same as *Top-Left panel* but with  $k_B T'_\gamma = 100$  eV,  $\Gamma = 300$ . *Bottom-Left panel:* Same as as *Top-Left panel* but with  $k_B T'_\gamma = 30$  eV,  $\Gamma = 300$ .

tions for  $\tau_{\text{initial}} = 5$ ,  $k_B T'_\gamma = 100$  eV,  $\gamma'_e \sim 2$ . For  $N_{\text{th}} = 50, 500$ , there is a power-law spectrum above the peak energy for  $\sim 2$  decades, with  $f_\nu \propto \nu^{-1.41}$  for  $N_{\text{th}} = 50$  and  $f_\nu \propto \nu^{-0.59}$  for  $N_{\text{th}} = 500$ . In the bottom-right panel, we show electron re-heating simulations for  $\tau_{\text{initial}} = 5$ ,  $k_B T'_\gamma = 100$  eV,  $\gamma'_e \sim 50$ . For  $N_{\text{th}} = 5, 50$ , there is a power-law spectrum above the peak energy for  $\sim 2$  decades, with  $f_\nu \propto \nu^{-1.00}$  for  $N_{\text{th}} = 5$  and  $f_\nu \propto \nu^{-0.44}$  for  $N_{\text{th}} = 50$ .

In summary, the main finding of considering electron re-heating is that there is only a  $f_\nu \propto \nu^{-1}$  spectrum above the peak energy if a specific number of electron re-heating events are considered. If too few electron re-heating events are considered, there is still a sharp drop in  $f_\nu$  after the peak energy and if too many electron re-heating events are considered, the high-energy spectrum will be shallower than  $f_\nu \propto \nu^{-1}$ . We also point out that the re-heating simulations in Figure 5 with a spectrum close to  $f_\nu \propto \nu^{-1}$  peak at  $\sim 100$  keV and the high-energy spectrum for these simulations extends to at least 10 MeV, in agreement with the prompt emission observations.

## 5 DISCUSSION OF RESULTS FOR THE COMPTONIZATION OF BB PHOTONS

In this section, we first discuss an energy requirement the electrons must satisfy to have enough energy to transfer to the photons to produce a power-law spectrum above the peak-energy. This energy requirement is a necessary, but not a sufficient condition, to explain the production of a power-law spectrum above the peak-energy. To give a more detailed explanation for the simulation results, we calculate the number of photons upscattered to higher energies in a simulation and compare this to the number of photons needed to be upscattered to produce a power-law spectrum. After this calculation, we discuss the interpretation for the drop in  $f_\nu$  by  $\sim 2$  orders of magnitude, immediately after the peak energy  $E_{\text{pk}}$ , for the simulations with  $k_B T'_\gamma \sim 30$  eV – 300 eV, one heating event, and  $\tau_{\text{initial}} = 2$ . We also discuss the interpretation of the simulations with  $k_B T'_\gamma = 30$  eV and  $\tau_{\text{initial}} 8, 16$ , which show a power-law spectrum above  $E_{\text{pk}}$ . We then apply this interpretation to the electron re-heating simula-



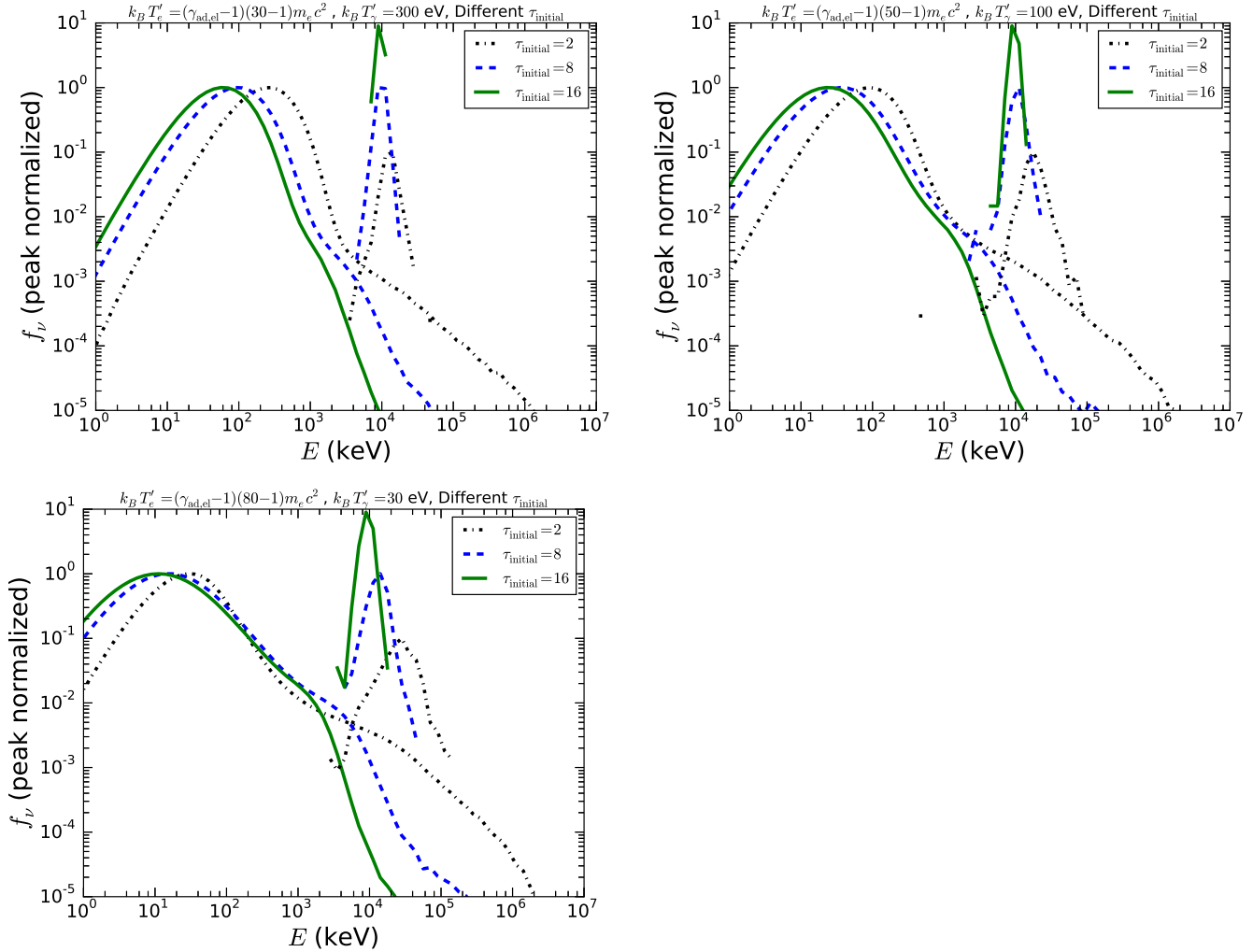


**Figure 4.** *Top-Left panel:* Simulation results for the Comptonization of seed BB photons with  $k_B T_\gamma' = 300$  eV,  $\Gamma = 300$  with MB electrons with initial  $\gamma_e' \sim 30$  and  $\tau_{\text{initial}} = 2, 8, 16$ . The photon spectra are peak normalized and the electron spectra (spectra in the top right) are shifted by a factor of 10 for each  $\tau_{\text{initial}}$  to better see if there is any change as  $\tau_{\text{initial}}$  becomes larger. For both the photons and the electrons, we are plotting their energy spectrum  $f_\nu = EN_E$ . *Top-Right panel:* Same as *Top-Left panel*, but with  $k_B T_\gamma' = 100$  eV,  $\Gamma = 300$  and MB electrons with initial  $\gamma_e' \sim 50$ . *Bottom-Left panel:* Same as *Top-Left panel*, but with  $k_B T_\gamma' = 30$  eV,  $\Gamma = 300$  and MB electrons with initial  $\gamma_e' \sim 80$ . The  $\tau_{\text{initial}} = 8, 16$  simulations in the *Bottom-Left panel* display a power-law with a spectrum  $f_\nu \propto \nu^{-1.2}$ .

tions with  $k_B T_\gamma' = 100$  eV, 300 eV to estimate how many electron reheating events it takes to produce a power-law spectrum above  $E_{\text{pk}}$ . Lastly, we discuss the dependence of the simulation results on the photon to electron ratio.

### 5.1 Energy Requirement for Power-Law Spectrum

In order to produce a power-law spectrum above the peak-energy, the electrons must have enough energy to transfer to the photons so they can populate a high-energy tail. A power-law spectrum can develop if the energy of a significant fraction of the photons near the BB peak-energy,  $\sim 1/2$ , can be increased by a factor  $\sim 2$ . Taking the number of photons near the BB peak to be  $\sim N_\gamma$  (most of the photons are near the peak), the energy requirement the electrons must satisfy is

$$N_e m_e c^2 \gamma_e' \gtrsim 2(N_\gamma/2)k_B T_\gamma' \quad (10)$$

When considering  $k_B T_\gamma' = 300$  eV and  $k_B T_\gamma' = 100$  eV, we considered  $\gamma_e' \sim 30$  and  $\gamma_e' \sim 50$ , respectively. For these two cases, for  $N_\gamma/N_e \sim 10^5$  (as observed for the GRB prompt emission), the electrons just meet the energy requirement, making the production of a power-law spectrum difficult (in agreement with the results presented in the top two panels of Figure 4). When considering  $k_B T_\gamma' = 30$  eV, we considered  $\gamma_e' \sim 80$ . For this case, the energy in the electrons is  $\sim 10$  larger than the energy that needs to be transferred to the photons. Thus, the electrons have enough energy to transfer to the photons to produce a power-law spectrum for this case, in agreement with the results presented in the bottom-left panel of Figure 4.

We now discuss a more detailed calculation to understand and interpret our simulation results.

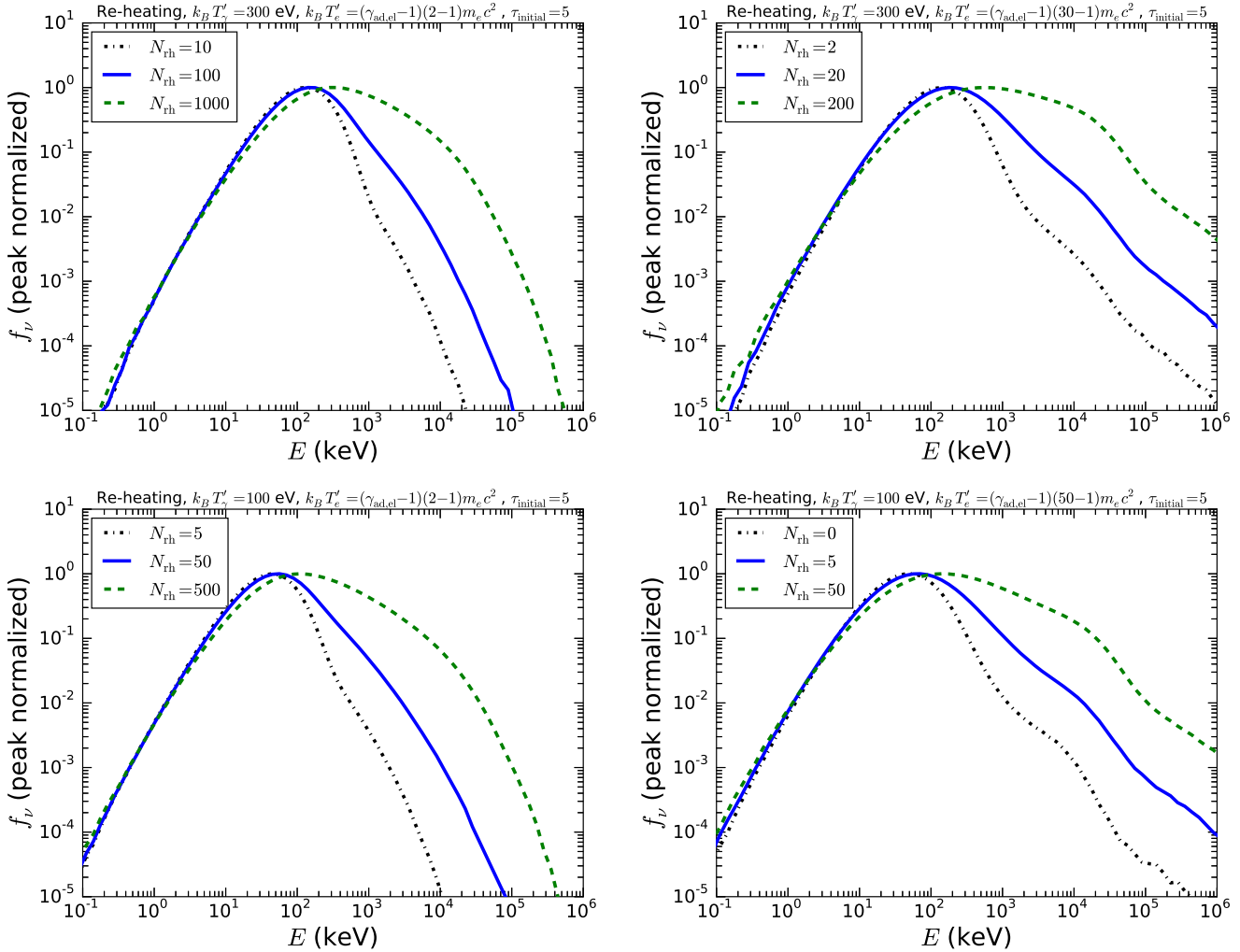


**Figure 5.** *Top-left Panel:* Simulation results for the Comptonization of seed BB photons with  $k_B T'_\gamma = 300$  eV,  $\Gamma = 300$  with mildly relativistic electrons with initial  $\gamma'_e \sim 2$ ,  $\tau_{\text{initial}} = 5$ , and  $N_{\text{rh}} = 10, 100, 1000$  electron re-heating events. Above  $E_{\text{pk}}$ ,  $f_\nu \propto \nu^{-1.43}$  for  $N_{\text{rh}} = 100$  for  $\sim 2$  decades in energy. *Top-right Panel:* Same as top-left panel, but with  $\gamma'_e \sim 30$  and  $N_{\text{rh}} = 2, 20, 200$  electron re-heating events. Above  $E_{\text{pk}}$ ,  $f_\nu \propto \nu^{-1.06}$  for  $N_{\text{rh}} = 20$  for  $\sim 2$  decades in energy. *Bottom-left Panel:* Simulation results for the Comptonization of seed BB photons with  $k_B T'_\gamma = 100$  eV,  $\Gamma = 300$  with mildly relativistic electrons with initial  $\gamma'_e \sim 2$ ,  $\tau_{\text{initial}} = 5$ , and  $N_{\text{rh}} = 5, 50, 500$  electron re-heating events. Above  $E_{\text{pk}}$ ,  $f_\nu \propto \nu^{-1.41}$  for  $N_{\text{rh}} = 50$  for  $\sim 2$  decades in energy. *bottom-right Panel:* Same as top-left panel, but with  $\gamma'_e \sim 50$  and  $N_{\text{rh}} = 0, 5, 50$  electron re-heating events. Above  $E_{\text{pk}}$ ,  $f_\nu \propto \nu^{-1.00}$  for  $N_{\text{rh}} = 5$  for  $\sim 2$  decades in energy.

## 5.2 Discussion of MC Simulation Results with One Heating Event

To understand our MC simulation results, we need to determine the number of photons that need to be upscattered to energies larger than  $E_{\text{pk}}$  to produce a power-law spectrum. We refer to this quantity as  $N_{\text{pl}}$ . We then compare  $N_{\text{pl}}$  to the total number of photons that are upscattered to energies larger than  $E_{\text{pk}}$  in a MC simulation, which is given by the number of electrons in a simulation,  $N_e$ , multiplied by  $N_{\text{Comp}}$ .  $N_{\text{Comp}}$  represent the number of scatterings it takes to cool an electron to a critical  $\gamma'_e$  at which Comptonization is no longer important. Thus, in order to produce a power-law above  $E_{\text{pk}}$ , we need the condition

$$N_e N_{\text{Comp}} \gtrsim N_{\text{pl}} \quad (11)$$

to be satisfied. We now estimate  $N_{\text{pl}}$  and  $N_{\text{Comp}}$  for our MC simulations.

### 5.2.1 Estimating $N_{\text{pl}}$

The number of photons in some bin with energy  $E$ , denoted as  $N_E$ , is given by

$$N_E = \frac{N_{\text{pk}}}{E_{\text{pk}}} \left( \frac{E}{E_{\text{pk}}} \right)^{-\beta-1}. \quad (12)$$

In this equation,  $N_{\text{pk}}$  is the number of photons at  $E_{\text{pk}}$  and the spectral index  $\beta$  is defined in the  $f_\nu$  sense, i.e.  $f_\nu \propto \nu^{-\beta}$ . To determine the total number of photons needed to produce a power-law above  $E_{\text{pk}}$ , we integrate  $N_E dE$  (sum over all the

bins) from  $E_{\text{pk}}$  to infinity:

$$N_{\text{pl}} = \int_{E'_{\text{pk}}}^{\infty} \frac{N_{\text{pk}}}{E_{\text{pk}}} \left( \frac{E}{E_{\text{pk}}} \right)^{-\beta-1} dE = \frac{N_{\text{pk}}}{\beta}. \quad (13)$$

For the prompt emission, the typical high-energy spectral index is  $\beta = 1.2$  (Preece et al. 2000). Thus, we approximate  $N_{\text{pl}} \sim N_{\text{pk}}$ . Since the majority of the photons in a simulation are near the peak of the BB spectrum, we approximate  $N_{\text{pl}} \sim N_{\text{pk}} \sim N_{\gamma}$ . With this result for  $N_{\text{pl}}$ , we can rewrite the condition to produce a power-law above  $E_{\text{pk}}$  (Equation 11) in terms of the photon to electron ratio ( $N_{\gamma}/N_e$ ):

$$N_{\text{Comp}} \gtrsim \frac{N_{\gamma}}{N_e} \sim 1 \times 10^5. \quad (14)$$

In the above expression, we used  $N_{\gamma}/N_e = 10^5$  for our MC simulations (Equation 2).

### 5.2.2 Condition for electron $\gamma'_e$ at which Comptonization is no longer important

The Compton- $Y$  parameter determines if the energy of a photon will change significantly after undergoing multiple scatterings with electrons in an optically thick medium. The expression for the Compton- $Y$  parameter is (Rybicki & Lightman 1979)

$$Y = 2\tau_{\text{initial}} \times \max \left[ \frac{4k_B T'_e}{m_e c^2}, \frac{4}{3} [(\gamma'_e)^2 - 1] \right], \quad (15)$$

where  $2\tau_{\text{initial}}$  is the average number of scatterings for each photon (Bégué et al. 2013) and the average fractional change of energy for a photon after a scattering event is either  $4k_B T'_e/m_e c^2$  (for mildly-relativistic or sub-relativistic electrons) or  $(4/3)[(\gamma'_e)^2 - 1]$  (for relativistic electrons), depending on the  $\gamma'_e$  of the electron. We take the transition from relativistic to mildly-relativistic speeds to occur at  $\gamma'_e = 2$ .

The condition Compton- $Y \gtrsim 1$  needs to be satisfied for Comptonization to be important. At the start of our MC simulations, Compton- $Y > 1$  since both  $2\tau_{\text{initial}}$  (we consider  $\tau_{\text{initial}} \geq 2$ ) and  $\max[4k_B T'_e/m_e c^2, (4/3)[(\gamma'_e)^2 - 1]]$  (we consider  $\gamma'_e \geq 2$ ) are larger than one. However, as the simulations proceed, since  $N_{\gamma} \gg N_e$ , the electrons may cool to a point where Comptonization is no longer important. The critical condition at which Comptonization is no longer important is given by

$$2\tau_{\text{initial}} \times \frac{4k_B T'_e}{m_e c^2} \sim 1. \quad (16)$$

Entering  $k_B T'_e \sim m_e c^2 (\gamma'_{e,\text{Comp}} - 1)$ , where  $\gamma'_{e,\text{Comp}}$  is the electron Lorentz factor at which Comptonization is no longer important, we find

$$\gamma_{e,\text{Comp}} = 1 + \frac{1}{8\tau_{\text{initial}}}. \quad (17)$$

Thus,  $\gamma_{e,\text{Comp}} = 1.06$  for  $\tau_{\text{initial}} = 2$  and  $\gamma_{e,\text{Comp}} = 1.008$  for  $\tau_{\text{initial}} = 16$ . With the value for  $\gamma_{e,\text{Comp}}$ , we can now estimate  $N_{\text{Comp}}$ .

### 5.2.3 Estimating $N_{\text{Comp}}$

The final  $\gamma'_e$  ( $\gamma'_{e,f}$ ) of an electron after a scattering event can be found from energy conservation (see Appendix E), which

is given by

$$\gamma'_{e,f} = \frac{E'_{\gamma,i} - E'_{\gamma,f} + m_e c^2 \gamma'_{e,i}}{m_e c^2}, \quad (18)$$

where  $E'_{\gamma,i}$  [ $E'_{\gamma,f}$ ] is the photon energy before [after] the scattering event and  $\gamma'_{e,i}$  is the electron Lorentz factor before the scattering event. As we discussed above, the average change of energy for a photon after a scattering event depends on whether  $\gamma'_e > 2$  or  $\gamma'_e < 2$  (Rybicki & Lightman 1979):

$$E'_{\gamma,f} - E'_{\gamma,i} = \frac{4}{3} [(\gamma'_{e,i})^2 - 1] E'_{\gamma,i}, \quad \text{for } \gamma'_{e,i} > 2 \quad (19)$$

$$E'_{\gamma,f} - E'_{\gamma,i} = \frac{4k_B T'_e}{m_e c^2} E'_{\gamma,i}, \quad \text{for } \gamma'_{e,i} < 2. \quad (20)$$

Substituting these expressions for  $E'_{\gamma,f} - E'_{\gamma,i}$  into Equation 18, we can solve for the change in electron  $\gamma'_e$  after a scattering event in terms of  $E'_{\gamma,i}$  and  $\gamma'_{e,i}$ :

$$\gamma'_{e,f} - \gamma'_{e,i} = -\frac{4E'_{\gamma,i}}{3m_e c^2} [(\gamma'_{e,i})^2 - 1], \quad \text{for } \gamma'_{e,i} > 2 \quad (21)$$

$$\gamma'_{e,f} - \gamma'_{e,i} = -\frac{4E'_{\gamma,i}}{m_e c^2} [\gamma'_{e,i} - 1], \quad \text{for } \gamma'_{e,i} < 2. \quad (22)$$

In Equation 22, for  $\gamma'_{e,i} < 2$ , we used  $k_B T'_e \sim m_e c^2 (\gamma'_{e,i} - 1)$  for the electron temperature. If we define the change in electron  $\gamma'_e$  per scattering as  $d\gamma'_e/dN$ , we can re-write Equation 21 and Equation 22 in differential form:

$$\frac{d\gamma'_e}{dN} = -\frac{4E'_\gamma}{3m_e c^2} [(\gamma'_e)^2 - 1], \quad \text{for } \gamma'_e > 2 \quad (23)$$

$$\frac{d\gamma'_e}{dN} = -\frac{4E'_\gamma}{m_e c^2} [\gamma'_e - 1], \quad \text{for } \gamma'_e < 2. \quad (24)$$

In the above expressions,  $E'_\gamma$  represents the energy of the photon in the jet-comoving frame before the scattering event. Solving these differential equations, we find

$$N_{\text{Cool,Rel}} = \frac{3m_e c^2}{8E'_\gamma} \ln \left[ \frac{(\gamma'_{e,\text{MR}} + 1)(\gamma'_{e,i} - 1)}{(\gamma'_{e,\text{MR}} - 1)(\gamma'_{e,i} + 1)} \right], \quad \text{for } \gamma'_{e,i} > 2 \quad (25)$$

$$N_{\text{Cool,MR}} = \frac{m_e c^2}{4E'_\gamma} \ln \left[ \frac{(\gamma'_{e,i} - 1)}{(\gamma'_{e,\text{Comp}} - 1)} \right], \quad \text{for } \gamma'_{e,i} \leq 2. \quad (26)$$

In Equation 25,  $N_{\text{Cool,Rel}}$  represents the number of scatterings it takes to cool a relativistic electron with  $\gamma'_{e,i} > 2$  to  $\gamma'_{e,\text{MR}} = 2$ . After an electron cools below  $\gamma'_{e,\text{MR}} = 2$ ,  $N_{\text{Cool,MR}}$  represents the number of scatterings it takes to cool a mildly-relativistic (MR) electron from  $\gamma'_{e,i} \leq 2$  to  $\gamma'_{e,\text{Comp}}$ .

For our simulations, we considered  $\gamma'_{e,i} \geq 2$ . If we consider  $\gamma'_{e,i} > 2$ , to compute  $N_{\text{Comp}}$ , we first need to compute the number of scatterings it takes to cool an electron to  $\gamma'_{e,\text{MR}} = 2$  (Equation 25). Then, we need to compute the number of scatterings it takes to cool an electron with  $\gamma'_{e,i} = 2$  to  $\gamma'_{e,\text{Comp}}$  (Equation 26). Thus, the number of scatterings it takes to cool a relativistic electron to  $\gamma'_{e,\text{Comp}}$  (defined as  $N_{\text{Comp,Rel}}$ ) is

$$N_{\text{Comp,Rel}} = N_{\text{Cool,Rel}}(\gamma'_{e,i} > 2) + N_{\text{Cool,MR}}(\gamma'_{e,i} = 2). \quad (27)$$

On the other hand, for a mildly-relativistic electron with  $\gamma'_{e,i} \leq 2$ , the number of scatterings it takes to cool an electron from  $\gamma'_{e,i}$  to  $\gamma'_{e,\text{Comp}}$  (defined as  $N_{\text{Comp,MR}}$ ) is simply found by computing  $N_{\text{Cool,MR}}$  (Equation 26). We give a summary of the values of  $N_{\text{Comp}}$  for the simulations we presented in Figures 2-4 in Table 2. When using Equation 25 and 26 to calculate  $N_{\text{Cool,Rel}}$  and  $N_{\text{Cool,MR}}$ , we assume  $E'_\gamma \sim k_B T'_\gamma$ , i.e. that the electrons cool mostly by scattering photons near the BB

	$N_{\text{Cool,MR}}(\gamma'_{e,i} = 2)$ $\tau_{\text{initial}} = 2$	$N_{\text{Cool,MR}}(\gamma'_{e,i} = 2)$ $\tau_{\text{initial}} = 16$	$N_{\text{Cool,Rel}}(\gamma'_{e,i} > 2)$
$k_B T'_\gamma = 30$ eV	$\sim 10^4$	$\sim 2 \times 10^4$	$\sim 7 \times 10^3$ for $\gamma_{e,i} = 80$
$k_B T'_\gamma = 100$ eV	$\sim 3 \times 10^3$	$\sim 6 \times 10^3$	$\sim 2 \times 10^3$ for $\gamma_{e,i} = 50$
$k_B T'_\gamma = 300$ eV	$\sim 10^3$	$\sim 2 \times 10^3$	$\sim 7 \times 10^2$ for $\gamma_{e,i} = 30$

**Table 2.** Values of  $N_{\text{Comp}}$  for the simulations we presented in Figures 2-4.  $N_{\text{Comp,MR}}$  and  $N_{\text{Comp,Rel}}$  were calculated with Equation 26 and Equation 27, respectively.

peak. This is not a bad approximation since most of the photons are near the BB peak.

#### 5.2.4 Interpretation of MC Simulation Results with One Heating Event

From the estimates we provided in Table 2 for  $N_{\text{Comp}}$  at  $\tau_{\text{initial}} = 2$ , for  $k_B T'_\gamma \sim 30$  eV – 300 eV and initial  $\gamma'_e \sim 2 - 80$ ,  $N_{\text{Comp}} \sim 2000 - 10000 \ll (N_\gamma/N_e)$  (Equation 14). Thus, not enough photons are upscattered to energies above  $E_{\text{pk}}$  to produce a power-law spectrum. The fraction of photons that can be upscattered to energies larger than  $E_{\text{pk}}$  is given by

$$\text{Fraction of upscattered photons} = \frac{N_e N_{\text{Comp}}}{N_\gamma} = \frac{N_{\text{Comp}}}{(N_\gamma/N_e)}, \quad (28)$$

where  $N_e N_{\text{Comp}}$  is the total number of photons upscattered to energies larger than  $E_{\text{pk}}$  and  $N_\gamma$  is the number of photons near the peak of the BB spectrum. For  $\tau_{\text{initial}} = 2$ ,  $N_{\text{Comp}}/[N_\gamma/N_e] \sim 10^{-2}$ . Since only  $\sim 10^{-2}$  of the photons near the BB peak are upscattered to higher energies, this result explains why  $f_\nu$  drops by  $\sim 2$  orders of magnitude and then a power-law spectrum begins to develop (Figures 2-3).

We now apply our analytical estimates to the simulation results for  $\tau_{\text{initial}} = 16$  presented in Figure 4. For  $k_B T'_\gamma \sim 100$  eV – 300 eV and  $\tau_{\text{initial}} = 16$ ,  $N_{\text{Comp}} \sim 3000 - 6000 < N_\gamma/N_e$  (Table 2). Thus, we do not expect a power-law spectrum to form above the peak energy, in agreement with the simulation results in Top-Left and Top-Right panels of Figure 4. For  $k_B T'_\gamma = 30$  eV and  $\tau_{\text{initial}} = 16$ ,  $N_{\text{Comp}} \sim 2 \times 10^4$  (Table 2). Since  $N_{\text{Comp}}$  is less than  $N_\gamma/N_e$  by a factor of 5, we do not expect a power-law spectrum to form above  $E_{\text{pk}}$ . However, our analytical estimate assumes that the electrons only cool, and does not consider the possibility that an electron can gain energy by interacting with an energetic photon. If the  $\gamma'_e$  of the electron rises to  $\gamma'_e \sim 2$ , it can upscatter  $\sim 20000$  more photons to higher energies since  $N_{\text{Cool,MR}} \sim 20000$  for  $k_B T'_\gamma = 30$  eV,  $\gamma'_e = 80$ , and  $\tau_{\text{initial}} = 16$  (Table 2). In Figure 6, we show the evolution of  $\gamma'_e$  for 3 electrons in the simulation. Initially, the 3 electrons cool from  $\gamma'_e = 80$  to  $\gamma'_e \sim 1$ . However, there are  $\sim 5$  instances where the  $\gamma'_e$  of the electron rises to  $\gamma'_e \sim 2$ . Thus, the number of photons that are upscattered to larger energies is increased by  $\sim 5$ , which give us  $N_{\text{Comp}} \sim N_\gamma/N_e$  (Equation 14), and explains why the  $\tau_{\text{initial}} = 16$  simulations in the Bottom-Left panel of Figure 4 show a power-law spectrum above  $E_{\text{pk}}$ .

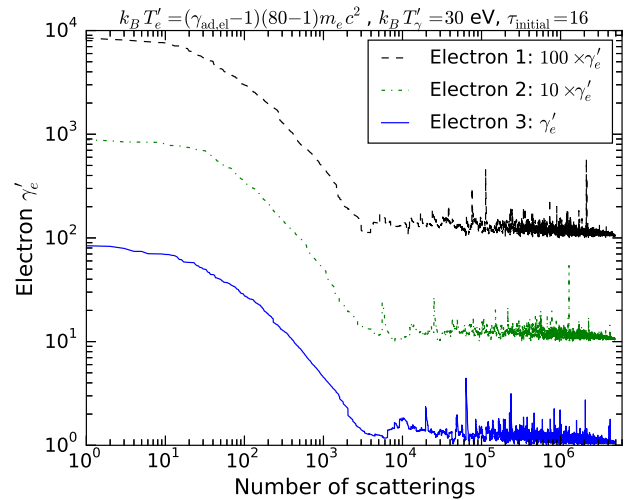


**Figure 6.** Evolution of  $\gamma'_e$  for 3 electrons from the  $\tau_{\text{initial}} = 16$  simulations shown in the Bottom-Left panel of Figure 4. The  $\gamma'_e$  of the electrons were offset by a factor of 10 to better see the evolution of  $\gamma'_e$  for each electron. Each of the spikes for  $\gamma'_e$  represents an episode when an electron interacts with an energetic photon, causing the energy of the electron to increase by a large factor.

### 5.3 Discussion of MC Simulation Results with Electron Reheating

In this subsection, we use the results for  $N_{\text{pl}}$  and  $N_{\text{Comp}}$  to understand the electron re-heating simulations with  $k_B T'_\gamma = 100$  eV - 300 eV presented in Figure 5. We estimate  $N_{\text{rh,min}}$ , the minimum number of re-heating events needed to produce a power-law spectrum above  $E_{\text{pk}}$ .

#### 5.3.1 Estimating $N_{\text{rh,min}}$

With  $N_{\text{rh}}$  electron re-heating events, the number of photons that can be upscattered to higher energies is  $\sim N_{\text{rh}} N_e N_{\text{Comp}}$ .  $N_{\text{rh,min}}$  is found by the condition where just enough photons are upscattered to energies larger than  $E_{\text{pk}}$  to produce a power-law spectrum, i.e.

$$N_{\text{rh,min}} N_e N_{\text{Comp}} = N_{\text{pl}}. \quad (29)$$

Using the result  $N_{\text{pl}} \sim N_\gamma$ , the condition for  $N_{\text{rh,min}}$  can be re-written in terms of the photon to electron ratio:

$$N_{\text{rh,min}} \sim \frac{N_\gamma/N_e}{N_{\text{Comp}}}. \quad (30)$$

For  $k_B T'_\gamma = 300$  eV and  $\gamma'_{e,i} \sim 2 - 30$ ,  $N_{\text{Comp}} \sim 2000 - 3000$  (Table 2); thus we estimate  $N_{\text{rh,min}} \sim 30 - 50$ .  $N_{\text{rh,min}}$  is within

a factor of a few of the simulations in the top panels of Figure 5, which show a power-law above the peak-energy for  $N_{\text{rh}} \sim 20 - 100$ . For  $k_B T'_\gamma = 100$  eV and  $\gamma'_{e,i} \sim 2 - 50$ ,  $N_{\text{Comp}} \sim 5000 - 8000$  (Table 2); thus we estimate  $N_{\text{rh,min}} \sim 10 - 20$ .  $N_{\text{rh,min}}$  is within a factor of a few of the simulations in the bottom panels of Figure 5, which show a power-law above the peak-energy for  $N_{\text{rh}} \sim 5 - 50$ .

#### 5.4 Dependence of Comptonization of Seed BB Simulation Results on $N_\gamma/N_e$

In this subsection, we perform a quick set of simulations at  $\tau_{\text{initial}} = 2$  to explore the dependence of the simulation results on  $N_\gamma/N_e$ . In the left panel (right panel) of Figure 7, we show simulation results for  $k_B T'_\gamma = 300$  eV,  $\Gamma = 300$ ,  $N_\gamma/N_e = 10^2, 10^3, 10^4, 10^5$ ,  $\tau_{\text{initial}} = 2$ , and mono-energetic electrons with initial  $\gamma'_e = 2$  ( $\gamma'_e = 30$ ). For  $N_\gamma/N_e = 10^2$  we considered  $N_e = 10^6$ , for  $N_\gamma/N_e = 10^3$  we considered  $N_e = 10^5$ , etc. This was done to keep  $N_\gamma = 10^8$  so that the simulation output spectrum can have more photons and thus a higher signal to noise. For initial  $\gamma'_e = 2$  (left panel of Figure 7), the spectrum shows a sharp drop above the peak energy for  $N_\gamma/N_e = 10^4$ . For  $N_\gamma/N_e = 10^3$ , the spectrum shows a power-law with  $f_\nu \propto \nu^{-1.60}$  and for  $N_\gamma/N_e = 10^2$  the spectrum also shows a power-law with  $f_\nu \propto \nu^{-0.80}$ . For initial  $\gamma'_e = 30$  (right panel of Figure 7), the spectrum shows a sharp drop above the peak energy for  $N_\gamma/N_e = 10^4$ . For  $N_\gamma/N_e = 10^3$ , there is a power-law spectrum  $f_\nu \propto \nu^{-0.70}$  and for  $N_\gamma/N_e = 10^2$  the spectrum is very shallow. The difference in the simulation results with  $N_\gamma/N_e$  can be understood from an energetics perspective. Equation 10, the minimum energy the electrons must have to transfer to the photons to produce a power-law spectrum, can be rewritten in terms of the photon to electron ratio:

$$\frac{m_e c^2 \gamma'_e}{N_\gamma/N_e} \gtrsim k_B T'_\gamma. \quad (31)$$

Thus, for a fixed  $k_B T'_\gamma$ , an increase in  $N_\gamma/N_e$  makes it more difficult to produce a power-law spectrum above the peak-energy, as demonstrated in both panels of Figure 7. These results highlight the strong dependence of the simulation results on  $N_\gamma/N_e$  and the importance of performing simulations with  $N_\gamma/N_e = 10^5$ .

Lastly, we note that Lazzati & Begelman (2010) also show a couple of simulation results for mono-energetic electrons with  $\gamma'_e = 2$ ,  $\tau_{\text{initial}} = 2$ , and  $N_\gamma/N_e = 10^4$  in their Figures 5-6. Their results for  $N_\gamma/N_e = 10^4$  also show a significant dip above the peak energy by a factor  $\sim 50$ . However, our simulation results in the left panel of Figure 7 for  $\gamma'_e = 2$  with  $N_\gamma/N_e = 10^4$  display a drop in  $f_\nu$  above  $E_{\text{pk}}$  by a factor  $\sim 100$ . This difference in the dip in  $f_\nu$  above the peak energy can be explained by the fact that Lazzati & Begelman (2010) considered a value for  $k_B T'_\gamma$  smaller than the  $k_B T'_\gamma$  value we considered by a factor of 2. Since  $N_{\text{Cool,MR}} \propto 1/E'_\gamma$  (Equation 26), a smaller value for  $k_B T'_\gamma$  by a factor of 2 implies that twice as many photons will be upscattered to larger energies (Equation 28). Thus, the  $N_\gamma/N_e = 10^4$  presented in Lazzati & Begelman (2010) are consistent with our analytical estimates and with our simulation results for  $N_\gamma/N_e = 10^4$ .

## 6 COMPTONIZATION OF SYNCHROTRON $F_\nu \propto \nu^{-1/2}$ SPECTRUM

In the previous sections, we considered the scenario where all the electrons were initially piled-up at  $\gamma'_e = \gamma_{\text{SA}}$ , where the optical depth to synchrotron self-absorption is 1. However, even when a system is optically thick to Thomson scattering as we consider, it is possible for the system to be optically-thin to synchrotron absorption. In this section, we consider a scenario where the synchrotron emission is initially optically thin. Then, we use our code to study how Comptonization modifies the photon spectrum produced by the synchrotron emission.

The situation we consider is the following. Initially, we take the electrons to be accelerated to a power-law distribution  $(\gamma'_i)^{-p}$  with  $\gamma'_i \gg \gamma'_{\text{SA}}$ , where  $\gamma'_i$  is the electron Lorentz factor where the power-law begins. Unless the magnetic field is very small, for typical GRB parameters, the electrons are expected to be in the fast cooling regime. In this regime, the electrons produce a  $f_\nu \propto \nu^{-1/2}$  synchrotron spectrum (Ghisellini et al. 2000). The electrons then continue to cool by emitting synchrotron photons until their Lorentz factor becomes  $\gamma'_{\text{SA}}$ . For electron Lorentz factors  $\gamma'_e \leq \gamma'_{\text{SA}}$ , although the electrons cannot cool via synchrotron emission, they can cool by IC scattering photons. To model this scenario, we consider a seed photon spectrum  $f_\nu \propto \nu^{-1/2}$ , instead of a BB spectrum. We then perform MC simulations to study how Comptonization modifies a  $f_\nu \propto \nu^{-1/2}$  photon spectrum. As before, we take all the electrons to initially be piled-up at  $\gamma'_e = \gamma'_{\text{SA}}$ . In the next subsection, we describe the input parameters we consider for these simulations.

### 6.1 Input Parameters for Simulations with Seed $f_\nu \propto \nu^{-1/2}$ Spectrum

For most of the input parameters, we considered the same values as those we considered for the Comptonization of a seed BB spectrum (discussed in Section 2.1). We considered  $\Gamma = 300$ ,  $L = 10^{52}$  ergs/sec,  $\tau_{\text{initial}} = 2, 5, 8, 16$ ,  $N_e = 10^3$ ,  $N_\gamma = 10^8$  to reach  $N_\gamma/N_e = 10^5$ , and  $N_{\text{collect}} = N_\gamma/3$ . For the  $f_\nu \propto \nu^{-1/2}$  seed spectrum, the input parameters are  $E'_{1,\gamma}$  and  $E'_{2,\gamma}$ , the energy where the  $f_\nu \propto \nu^{-1/2}$  spectrum begins and ends, respectively, in the jet-comoving frame. Thus, in the observer frame, the  $f_\nu \propto \nu^{-1/2}$  spectrum begins and ends at  $E_{1,\gamma} = \mathcal{D}E'_{1,\gamma}$  and  $E_{2,\gamma} = \mathcal{D}E'_{2,\gamma}$ . As we will discuss in the next subsection, the effect of Comptonizing a  $f_\nu \propto \nu^{-1/2}$  spectrum is to flatten it to  $f_\nu \propto \nu^0$ , reminiscent of the low-energy spectrum of the prompt emission. Since the observed  $f_\nu \propto \nu^0$  spectrum for the prompt emission extends from  $\lesssim 10$  keV to  $E_{\text{pk}} = 300$  keV, we considered  $E'_{1,\gamma} = 0.01$  eV and  $E'_{2,\gamma} = 300$  eV. For the electron distribution, we considered MB electrons with  $k_B T'_e \sim (2000 - 1)m_e c^2$ . We obtained  $\gamma'_e \sim 2000$  by setting  $\tau_{\text{sync}}^{\text{MB}} = 1$  in Equation 8. For  $E'_\gamma$  in Equation 8, we took 0.01 eV since most of the photons are at this energy for the  $f_\nu \propto \nu^{-1/2}$  photon spectrum we consider. Lastly, we note that we do not consider electron re-heating, i.e. the electrons are only accelerated once at the start of the simulations.

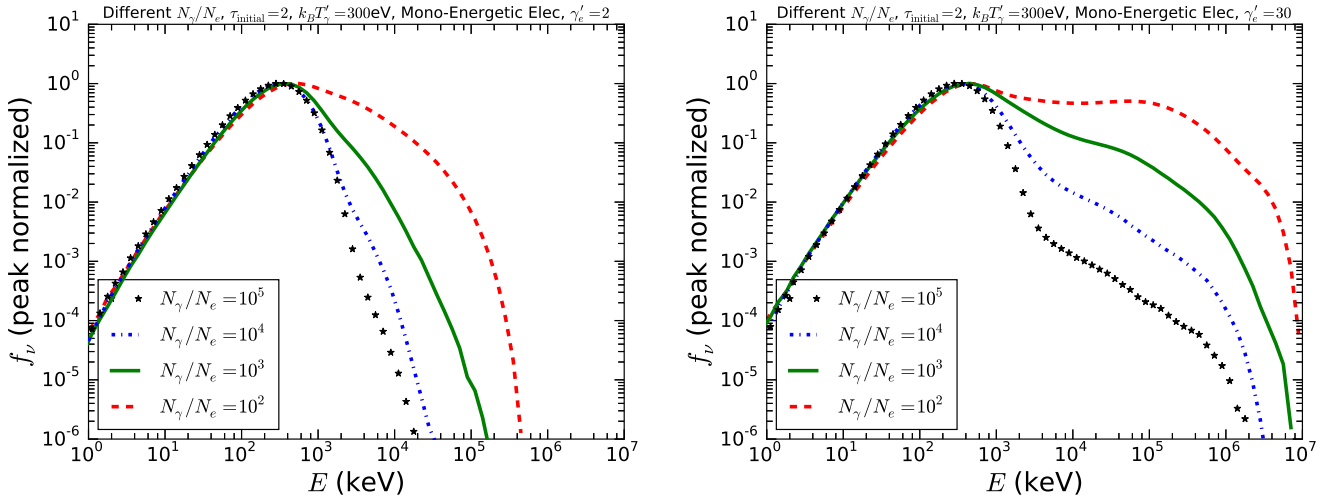


**Figure 7.** *Left Panel:* Simulation results for the Comptonization of seed BB photons with  $k_B T'_\gamma = 300$  eV,  $\Gamma = 300$  with mildly relativistic electrons with initial  $\gamma'_e = 2$ , four different values for the photon to electron ratio, and  $\tau_{\text{initial}} = 2$ . *Right Panel:* Same as Left Panel but with mono-energetic electrons with initial  $\gamma'_e = 30$ .

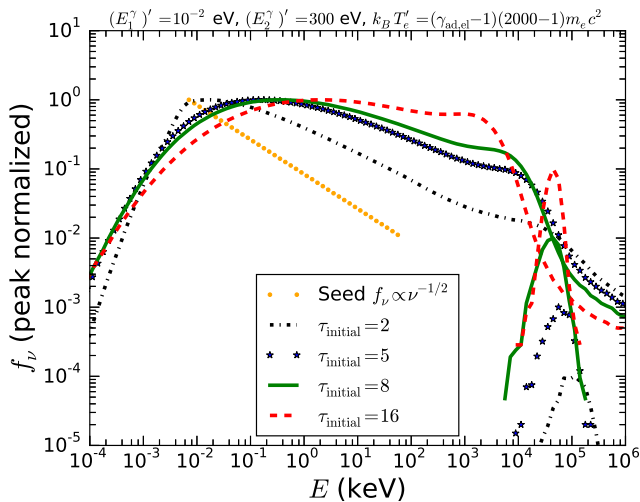


**Figure 8.** Simulation results for the Comptonization of a seed  $f_\nu \propto \nu^{-1/2}$  spectrum ( $E'_{1,\gamma} = 10^{-2}$  eV,  $E'_{2,\gamma} = 300$  eV) with MB electrons with  $k_B T'_e \sim (2000 - 1)m_e c^2$  and  $\tau_{\text{initial}} = 2, 5, 8, 16$ . As in Figure 4, the photon spectra are peak normalized and the electron spectra (spectra in the bottom right) are shifted by a factor of 10 for each  $\tau_{\text{initial}}$ .

## 6.2 Simulation Results for Comptonization of $f_\nu \propto \nu^{-1/2}$ Seed Spectrum

In Figure 8, we show the results for the Comptonization of a seed  $f_\nu \propto \nu^{-1/2}$  spectrum with  $E'_{1,\gamma} = 0.01$  eV,  $E'_{2,\gamma} = 300$  eV, MB electrons with  $k_B T'_e \sim (2000 - 1)m_e c^2$ , and  $\tau_{\text{initial}} = 2, 5, 8, 16$ . In addition, we also plot the energy spectrum  $f_\nu = EN_E$  of the kinetic energies of the electrons in the observer frame, i.e.  $m_e c^2(\gamma_{\text{ad,el}} - 1)(\gamma'_e - 1)\Gamma$ , at the end of each simulation. We will first discuss the results for the electron distributions. At the end of the  $\tau_{\text{initial}} = 2$  simulations, the electron distributions peak at  $k_B T'_e \sim 100$  keV (in the jet-comoving frame). As

$\tau_{\text{initial}}$  increases,  $k_B T'_e$  doesn't change by much; at the end of the  $\tau_{\text{initial}} = 16$  simulation  $k_B T'_e \sim 50$  keV. On the other hand, the photon spectrum changes significantly as  $\tau_{\text{initial}}$  increases. At the end of the  $\tau_{\text{initial}} = 2$  simulations, most of the photons in the seed spectrum are initially present. However, as  $\tau_{\text{initial}}$  increases, more and more photons begin to be upscattered to energies  $\sim 10^4$  keV. At the end of the  $\tau_{\text{initial}} = 16$ , the spectrum is flat from  $\sim 1$  keV to  $\sim 10^4$  keV. After  $\sim 10^4$  keV, the spectrum declines rapidly for all of the simulations. After the rapid decline, there are a significant number of photons with energies  $\gtrsim 10^5$  keV for all of the simulations. These photons remain at these energies since they are highly Klein-Nishina suppressed and cannot transfer their energy back to the electrons.

We now discuss the basic interpretation for the flattening of the spectrum as  $\tau_{\text{initial}}$  increases. From Equation 17, for  $\tau_{\text{initial}} = 16$ , the  $\gamma'_e$  at which Comptonization is no longer important is  $\gamma_{e,\text{Comp}} = 1.008$ . At the end of the  $\tau_{\text{initial}} = 16$  simulations,  $k_B T'_e \sim 50$  keV. Using  $k_B T'_e \sim m_e c^2(\gamma_e - 1)$ ,  $\gamma_e \sim 1.1 > \gamma_{e,\text{Comp}}$ . Thus, Comptonization is still important for the  $\tau_{\text{initial}} = 16$  simulations and the photons are still gaining energy from the electrons. The photons will gain energy from the electrons until they reach the energy of the electrons. For the seed  $f_\nu \propto \nu^{-1/2}$  spectrum, initially there are more photons at lower energies near  $E_{1,\gamma}$ . However, as  $\tau_{\text{initial}}$  increases, the additional scatterings allow for more photons at lower energies to be upscattered to higher energies and they also allow for more photons to reach the energy of the electrons. The spectrum flattens because more photons are being removed from lower energies and being placed at high energies near the energy of the electrons. If we considered  $\tau_{\text{initial}} > 16$ , if Compton-Y remains greater than 1, eventually all the photons will be upscattered to energies close to the energy of the electrons. The photon spectrum will no longer look flat, but will instead be peaked at the energy of the electrons.

Lastly, we note that although the simulation output

spectrum for  $\tau_{\text{initial}} = 16$  in Figure 8 is very similar to the low-energy spectrum for the prompt emission, these simulation results cannot explain it. The spectrum peaks at the energy of the electrons, which have an energy  $\sim 50$  keV in the jet-comoving frame and thus an energy  $\sim 50 \text{ keV} \times 300 \sim 10^4$  keV in the observer frame ( $\Gamma = 300$ ). In order for the spectrum to break at  $\sim 300$  keV in the observer frame, the electrons would need to have an energy  $\sim 1$  keV in the jet-comoving frame. In addition, once the  $f_\nu \propto \nu^0$  spectrum ends in Figure 8, the spectrum declines very rapidly, in disagreement with the observed  $f_\nu \propto \nu^{-1.2}$  for the prompt emission.

## 7 CONCLUSIONS

In this work, we presented our methodology for our MC photospheric code and our simulation results for a wide parameter space with a realistic photon to electron ratio  $N_\gamma/N_e = 10^5$ , as expected for the GRB prompt emission. Our goal was to determine if the photospheric process can explain the observed high-energy spectrum  $f_\nu \propto \nu^{-1.2}$  of the prompt emission. For these simulations, we considered the Comptonization of a seed BB spectrum. If electron re-heating is not considered, we determined that considering both low photon temperatures and large optical depths  $\sim 10 - 20$  is best for producing a power-law spectrum above the BB peak energy for the following two reasons: 1. low temperature photons cool electrons more slowly, allowing more photons to be upscattered to higher energies. 2. At larger optical depths, the average number of scatterings a photon experiences is larger, allowing for more photons to be upscattered to higher energies. On the other hand, the output spectrum for the cases we considered with higher photon temperatures and low optical depths display a sharp drop in  $f_\nu$  above the peak energy by  $\sim 2$  orders of magnitude. These cases require additional energy in the electrons and we demonstrated that if we consider electron re-heating, a power-law spectrum above the peak-energy can be produced.

One issue with the simulations with a low photon temperature and a large optical depth is that it is difficult to match the peak-energy of the prompt emission since adiabatic cooling of photons decreases the BB peak-energy by a large factor for large optical depths. For these simulations (lower-left panel of 4), the spectrum peaks at  $\sim 30$  keV, 10 times lower than the typical peak-energy of the prompt emission. On the other hand, when considering electron re-heating, we find simulation results with 1. peak-energy  $\sim 100$  keV 2. a power-law spectrum extending to at least 10 MeV 3. a spectral index similar to  $f_\nu \propto \nu^{-1.2}$ , all in agreement with the prompt emission observations. Thus, considering electron re-heating near the photosphere with a large photon temperature ( $\sim 100$  keV in the observer frame) may be the best solution for explaining the prompt emissions observations with the photospheric process. We note that the electron re-heating scheme we consider is a global re-heating mechanism since we re-accelerate all the electrons in our simulations after a re-heating episode. In GRBs, the heating mechanism is likely to be global, i.e. occurring throughout the causally connected part of the jet, since observations show that the conversion of jet energy to gamma-ray radiation is an efficient process.

We also performed photospheric simulations for differ-

ent values of  $N_\gamma/N_e$  and demonstrated that the simulation results have a strong dependence on the photon to electron ratio. This result highlights the importance of performing realistic photospheric simulations with  $N_\gamma/N_e = 10^5$ .

In addition, we also used our MC photospheric code to study how Comptonization modifies a  $f_\nu \propto \nu^{-1/2}$  seed spectrum, as expected for synchrotron when electrons are in the fast cooling regime. For large optical depths, the effect is to flatten the spectrum to  $f_\nu \propto \nu^0$ , reminiscent of the low-energy spectrum of the Band function. However, these simulation results cannot explain the low-energy spectrum of the prompt emission since the simulation output spectrum peaks at  $\sim 10^4$  keV, much larger than the  $\sim 300$  keV peak energy of the prompt emission. In addition, above the peak-energy, the spectrum declines very rapidly, in disagreement with the observed  $f_\nu \propto \nu^{-1.2}$  for the prompt emission.

## ACKNOWLEDGEMENTS

We thank the referee for a prompt and constructive referee report, which significantly improved the manuscript. The authors would like to thank Volker Bromm and Miloš Milosavljević for generously providing computational resources. R.S. would like to dedicate this work to Rodolfo Barnier Duran, who has been a good mentor and who has taught me a lot about GRBs. R.S. also thanks Davide Lazzati and Wenbin Lu for helpful discussions.

## REFERENCES

- Band D., et al., 1993, *ApJ*, 413, 281  
 Bégué D., Iyyani S., 2014, *ApJ*, 792, 42  
 Bégué D., Pe'er A., 2015, *ApJ*, 802, 134  
 Bégué D., Siutsou I. A., Vereshchagin G. V., 2013, *ApJ*, 767, 139  
 Chhotray A., Lazzati D., 2015, *ApJ*, 802, 132  
 Daigne F., Mochkovitch R., 2002, *MNRAS*, 336, 1271  
 Deng W., Zhang B., 2014, *ApJ*, 785, 112  
 Fan Y., Piran T., 2006, *MNRAS*, 369, 197  
 Gao H., Zhang B., 2015, *ApJ*, 801, 103  
 Ghisellini G., ed. 2013, Radiative Processes in High Energy Astrophysics Lecture Notes in Physics, Berlin Springer Verlag Vol. 873. ([arXiv:1202.5949](https://arxiv.org/abs/1202.5949)), doi:10.1007/978-3-319-00612-3, <http://adsabs.harvard.edu/abs/2013LNP...873.....G>  
 Ghisellini G., Celotti A., 1999, *ApJ*, 511, L93  
 Ghisellini G., Celotti A., Lazzati D., 2000, *MNRAS*, 313, L1  
 Giannios D., 2006, *A&A*, 457, 763  
 Giannios D., 2008, *A&A*, 480, 305  
 Giannios D., 2012, *MNRAS*, 422, 3092  
 Giannios D., Spruit H. C., 2005, *A&A*, 430, 1  
 Goodman J., 1986, *ApJ*, 308, L47  
 Gou L.-J., Fox D. B., Mészáros P., 2007, *ApJ*, 668, 1083  
 Granot J., Königl A., Piran T., 2006, *MNRAS*, 370, 1946  
 Ito H., Nagataki S., Matsumoto J., Lee S.-H., Tolstov A., Mao J., Dainotti M., Mizuta A., 2014, *ApJ*, 789, 159  
 Kaneko Y., Preece R. D., Briggs M. S., Paciesas W. S., Meegan C. A., Band D. L., 2006, *ApJS*, 166, 298  
 Kumar P., Zhang B., 2015, *Phys. Rep.*, 561, 1  
 Lazzati D., Begelman M. C., 2010, *ApJ*, 725, 1137  
 Lazzati D., Morsony B. J., Margutti R., Begelman M. C., 2013, *ApJ*, 765, 103  
 Liang E., Zhang B., Virgili F., Dai Z. G., 2007, *ApJ*, 662, 1111  
 Liang E.-W., Yi S.-X., Zhang J., Lü H.-J., Zhang B.-B., Zhang B., 2010, *ApJ*, 725, 2209

- Lundman C., Pe'er A., Ryde F., 2013, *MNRAS*, 428, 2430  
Mészáros P., Rees M. J., 2000, *ApJ*, 530, 292  
Mészáros P., Ramirez-Ruiz E., Rees M. J., Zhang B., 2002, *ApJ*, 578, 812  
Mizuta A., Nagataki S., Aoi J., 2011, *ApJ*, 732, 26  
Molinari E., et al., 2007, *A&A*, 469, L13  
Paczynski B., 1990, *ApJ*, 363, 218  
Pe'er A., 2008, *ApJ*, 682, 463  
Pe'er A., 2015, preprint ([arXiv:1504.02626](https://arxiv.org/abs/1504.02626))  
Pe'er A., Ryde F., 2011, *ApJ*, 732, 49  
Pe'er A., Mészáros P., Rees M. J., 2006, *ApJ*, 642, 995  
Piran T., 2004, *Reviews of Modern Physics*, 76, 1143  
Pozdnyakov L. A., Sobol I. M., Syunyaev R. A., 1983, *Astrophysics and Space Physics Reviews*, 2, 189  
Preece R. D., Briggs M. S., Malozzi R. S., Pendleton G. N., Paciasas W. S., Band D. L., 2000, *ApJS*, 126, 19  
Rees M. J., Mészáros P., 2005, *ApJ*, 628, 847  
Ruffini R., Siutsou I. A., Vereshchagin G. V., 2013, *ApJ*, 772, 11  
Rybicki G. B., Lightman A. P., 1979, *Radiative processes in astrophysics*. Wiley-Interscience, <http://adsabs.harvard.edu/abs/1979rpa..book.....R>  
Sari R., Narayan R., Piran T., 1996, *ApJ*, 473, 204  
Thompson C., 1994, *MNRAS*, 270, 480  
Thompson C., Mészáros P., Rees M. J., 2007, *ApJ*, 666, 1012  
Toma K., Wu X.-F., Mészáros P., 2011, *MNRAS*, 415, 1663  
Vereshchagin G. V., 2014, *International Journal of Modern Physics D*, 23, 30003  
Vurm I., Lyubarsky Y., Piran T., 2013, *ApJ*, 764, 143  
Wanderman D., Piran T., 2010, *MNRAS*, 406, 1944  
Wu X. F., Dai Z. G., Huang Y. F., Lu T., 2003, *MNRAS*, 342, 1131  
Xue R.-R., Fan Y.-Z., Wei D.-M., 2009, *A&A*, 498, 671  
Zhang B., 2014, *International Journal of Modern Physics D*, 23, 30002  
Zhang B., et al., 2007, *ApJ*, 655, 989

## APPENDIX A: CONVENTIONS FOR APPENDICES

In the appendices below, we describe the details of the algorithm we adopted for our MC Photospheric code. The algorithms in Appendices B1, B2, C1, C2, and D were adopted from the comprehensive IC/Compton scattering reference Pozdnyakov et al. (1983).

The conventions we describe here apply to all the Appendices below. All primed (un-primed) quantities are in the jet-comoving (observer) frame. A quantity with a subscript  $i$  (initial) [ $f$  (final)] refers to the quantity before [after] the scattering event. All the random numbers we draw are denoted by  $\xi$  and they are uniform random numbers in the interval 0 to 1. When referring to a vector  $\mathbf{A}$ , the vector is put in boldface and the magnitude of the vector is denoted by  $\|\mathbf{A}\|$ . Lastly,  $\hat{x}$ ,  $\hat{y}$ ,  $\hat{z}$  represent the unit vectors in Cartesian coordinates.

## APPENDIX B: INITIALIZATION OF ELECTRONS

### B1 Drawing Random Electron Directions

The momentum of an electron is given by  $\mathbf{p}'_e = \|\mathbf{p}'_e\|v'_1\hat{x} + \|\mathbf{p}'_e\|v'_2\hat{y} + \|\mathbf{p}'_e\|v'_3\hat{z}$ , where  $v'_1$ ,  $v'_2$ , and  $v'_3$  are the components of  $\mathbf{p}'_e$  in the x, y, and z directions, respectively. To draw a

random direction for an electron, draw two random numbers  $\xi_1$ ,  $\xi_2$  and use the expressions

$$\begin{aligned} v'_3 &= 2\xi_1 - 1 \\ v'_2 &= \sqrt{1 - (v'_3)^2} \sin(2\pi\xi_2) \\ v'_1 &= \sqrt{1 - (v'_3)^2} \cos(2\pi\xi_2). \end{aligned}$$

### B2 Drawing Electron Energy from MB and PL Distributions

#### B2.1 Maxwell Boltzmann Electrons

The dimensionless energy ( $n$ ) and the dimensionless momentum ( $\eta$ ) of an electron are given by  $n = k_B T'_e / (m_e c^2)$  and  $\eta = \|\mathbf{p}'_e\| / (m_e c)$ , where  $\|\mathbf{p}'_e\| = m_e c \beta'_e \gamma'_e$ . From the expression for  $\eta$ ,  $\gamma'_e = \sqrt{\eta^2 + 1}$  and  $\beta'_e = \eta / \gamma'_e$ . Pozdnyakov et al. (1983) present two algorithms for drawing  $\gamma'_e$  for an electron, depending on whether  $k_B T'_e$  is less than or larger than 150 keV.

If  $k_B T'_e < 150$  keV, draw two random numbers  $\xi_1$ ,  $\xi_2$ . First, calculate  $\xi'$  with the expression  $\xi' = -(3/2) \ln(\xi_1)$ . Then, test the acceptance-rejection condition  $\xi_2^2 < 0.151(1 + n\xi')^2 \xi'(2 + n\xi') \xi_1$ . If it is satisfied, set  $\eta = \sqrt{n\xi'(2 + n\xi')}$ ,  $\gamma'_e = \sqrt{\eta^2 + 1}$ , and  $\beta'_e = \eta / \gamma'_e$ . Otherwise, continue to draw new  $\xi_1$ ,  $\xi_2$  until the acceptance-rejection condition is satisfied.

If  $k_B T'_e \geq 150$  keV, draw four random numbers  $\xi_1$ ,  $\xi_2$ ,  $\xi_3$ ,  $\xi_4$ . Compute the quantities  $\eta' = -n \ln(\xi_1 \xi_2 \xi_3)$  and  $\eta'' = -n \ln(\xi_1 \xi_2 \xi_3 \xi_4)$  and test the acceptance-rejection condition  $(\eta'')^2 - (\eta')^2 > 1$ . If it is satisfied, set  $\eta = \eta'$ ,  $\gamma'_e = \sqrt{\eta^2 + 1}$ , and  $\beta'_e = \eta / \gamma'_e$ . Otherwise, continue to draw new  $\xi_1$ ,  $\xi_2$ ,  $\xi_3$ ,  $\xi_4$  until the acceptance-rejection condition is satisfied.

#### B2.2 Power-Law Distribution of Electrons

To draw  $\gamma'_e$  for an electron following a PL distribution, draw one random number  $\xi_1$  and calculate  $E' = m_e c^2 \gamma'_e$  with the expression

$$E' = [\xi_1 ((E'_2)^{1-p} - (E'_1)^{1-p}) + (E'_1)^{1-p}]^{1/(1-p)}.$$

Then, we set  $\gamma'_e = E' / (m_e c^2)$  and  $\beta_e = \sqrt{1 - (\gamma'_e)^{-2}}$ .

## APPENDIX C: INITIALIZATION OF PHOTONS

### C1 Photon Directions

The momentum of a photon is given by  $\mathbf{p}'_\gamma = (E'_\gamma/c)\Omega'_1\hat{x} + (E'_\gamma/c)\Omega'_2\hat{y} + (E'_\gamma/c)\Omega'_3\hat{z}$ , where  $\Omega'_1$ ,  $\Omega'_2$ , and  $\Omega'_3$  are the components of  $\mathbf{p}'_\gamma$  in the x, y, and z directions, respectively. To draw a random direction for a photon, draw two random numbers  $\xi_1$ ,  $\xi_2$  and use the expressions (same algorithm as in Appendix B1)

$$\begin{aligned} \Omega'_3 &= 2\xi_1 - 1 \\ \Omega'_2 &= \sqrt{1 - (\Omega'_3)^2} \sin(2\pi\xi_2) \\ \Omega'_1 &= \sqrt{1 - (\Omega'_3)^2} \cos(2\pi\xi_2). \end{aligned}$$



## C2 Photon Energies

### C2.1 BB Distribution

Draw four random numbers  $\xi_1, \xi_2, \xi_3, \xi_4$ . Then, determine  $\alpha$  such that

$$\alpha = \begin{cases} 1 & \text{if } 1.202\xi_1 < 1 \\ m & \text{if } \sum_1^{m-1} j^{-3} \leq 1.202\xi_1 < \sum_1^m j^{-3}. \end{cases}$$

Then, set  $E'_\gamma = -(k_B T'_\gamma / \alpha) \ln(\xi_2 \xi_3 \xi_4)$ .

### C2.2 Power-Law Distribution

To draw a photon power-law distribution with  $E'_{\gamma,1} < E < E'_{\gamma,2}$ , draw one random number  $\xi_1$  and set

$$E'_\gamma = [\xi_1((E'_{\gamma,2})^{1-p} - (E'_{\gamma,1})^{1-p}) + (E'_{\gamma,1})^{1-p}]^{1/(1-p)}.$$

The  $f_\nu$  photon spectrum is given by  $f_\nu \propto \nu^{1-p}$ .

## C3 Photon Propagation

In this subappendix, we calculate the new position of a photon in the observer frame after it has traveled a distance  $s'$  in the jet-comoving frame. We denote the initial [final] position of the photon in the observer frame as  $\mathbf{R}_i = R_{1,i}\hat{x} + R_{2,i}\hat{y} + R_{3,i}\hat{z}$  [ $\mathbf{R}_f = R_{1,f}\hat{x} + R_{2,f}\hat{y} + R_{3,f}\hat{z}$ ]. The time traveled by the photon in the jet-comoving frame ( $\Delta t'$ ) and the displacements of the photon in the jet-comoving frame in the x ( $\Delta R'_1$ ), y ( $\Delta R'_2$ ), and z ( $\Delta R'_3$ ) directions are given by

$$\begin{aligned} \Delta t' &= s'(R)/c \\ \Delta R'_1 &= s'(R)\Omega'_{1,i} \\ \Delta R'_2 &= s'(R)\Omega'_{2,i} \\ \Delta R'_3 &= s'(R)\Omega'_{3,i}, \end{aligned}$$

where  $\Omega'_{1,i}$  ( $\Omega'_{2,i}$ ) [ $\Omega'_{3,i}$ ] is the direction of the photon in the x (y) [z] direction before the scattering event.

From the bulk Lorentz factor of the jet, the speed of the jet divided by the speed of light is  $\beta_j = \sqrt{1 - \Gamma^{-2}}$ . The components of  $\beta_j$  in the x ( $\beta_{j,1}$ ), y ( $\beta_{j,2}$ ), and z ( $\beta_{j,3}$ ) directions are given by

$$\begin{aligned} \beta_{j,1} &= \beta_j \cos \phi \sin \theta \\ \beta_{j,2} &= \beta_j \sin \phi \sin \theta \\ \beta_{j,3} &= \beta_j \cos \theta. \end{aligned}$$

The angles  $\theta$  and  $\phi$ , corresponding to the photon position in spherical coordinates, can be found with the expressions  $\cos \theta = R_{3,i} / \sqrt{(R_{1,i})^2 + (R_{2,i})^2 + (R_{3,i})^2}$  and  $\tan \phi = R_{2,i} / R_{1,i}$ . With these results, we can Lorentz transform the displacements from the jet comoving frame to the observe frame with the

expressions

$$\begin{aligned} \Delta R_1 &= \Gamma\beta_{j,1}c\Delta t' + \left[1 + (\Gamma - 1)\frac{\beta_{j,1}^2}{\beta_j^2}\right]\Delta R'_1 + \\ &\quad \left[(\Gamma - 1)\frac{\beta_{j,1}\beta_{j,2}}{\beta_j^2}\right]\Delta R'_2 + \left[(\Gamma - 1)\frac{\beta_{j,1}\beta_{j,3}}{\beta_j^2}\right]\Delta R'_3 \\ \Delta R_2 &= \Gamma\beta_{j,2}c\Delta t' + \left[(\Gamma - 1)\frac{\beta_{j,2}\beta_{j,1}}{\beta_j^2}\right]\Delta R'_1 + \\ &\quad \left[1 + (\Gamma - 1)\frac{\beta_{j,2}^2}{\beta_j^2}\right]\Delta R'_2 + \left[(\Gamma - 1)\frac{\beta_{j,2}\beta_{j,3}}{\beta_j^2}\right]\Delta R'_3 \\ \Delta R_3 &= \Gamma\beta_{j,3}c\Delta t' + \left[(\Gamma - 1)\frac{\beta_{j,3}\beta_{j,1}}{\beta_j^2}\right]\Delta R'_1 + \\ &\quad \left[(\Gamma - 1)\frac{\beta_{j,3}\beta_{j,2}}{\beta_j^2}\right]\Delta R'_2 + \left[1 + (\Gamma - 1)\frac{\beta_{j,3}^2}{\beta_j^2}\right]\Delta R'_3. \\ \Delta t &= \Gamma\Delta t' + \Gamma\beta_{j,1}(\Delta R'_1/c) + \\ &\quad \Gamma\beta_{j,2}(\Delta R'_2/c) + \Gamma\beta_{j,3}(\Delta R'_3/c). \end{aligned}$$

In the above equation,  $\Delta t$  is the time it took the photon to travel a distance  $s'$  in the observer frame. The new position of the photon and the new distance of the photon from the central engine can be found with the equations

$$\begin{aligned} R_{1,f} &= R_{1,i} + \Delta R_1 \\ R_{2,f} &= R_{2,i} + \Delta R_2 \\ R_{3,f} &= R_{3,i} + \Delta R_3 \\ R &= \sqrt{(R_{1,f})^2 + (R_{2,f})^2 + (R_{3,f})^2}. \end{aligned}$$

## APPENDIX D: ELECTRON PHOTON SCATTERING INTERACTION

In this Appendix, we describe the algorithm from Chapter 9 of [Pozdnyakov et al. \(1983\)](#) for calculating the final energy ( $E'_{\gamma,f}$ ) and direction of a photon ( $\Omega'_{1,f}, \Omega'_{2,f}, \Omega'_{3,f}$ ) after a scattering event. The angle between the electron direction and photon direction before the scattering event is given by

$$\mu'_i = v'_{1,i}\Omega'_{1,i} + v'_{2,i}\Omega'_{2,i} + v'_{3,i}\Omega'_{3,i}.$$

With the angle  $\mu'_i$ , we can compute the dimensionless photon energy in the electron rest-frame, denoted as  $x'_i$ , with the expression

$$x'_i = 2\gamma'_{e,i}(E'_{\gamma,i}/m_e c^2)(1 - \mu'_i\beta'_{e,i}).$$

With  $x'_i$ , we can compute the cross-section for this interaction,  $\sigma(x'_i) = 2\pi r_e^2 \hat{\sigma}(x'_i)$ , where  $r_e = e^2/(m_e c^2)$  is the Classical electron radius,  $e$  is the electron charge, and  $\hat{\sigma}$  is calculated with the expression ([Pozdnyakov et al. 1983](#))

$$\hat{\sigma}(x'_i) = \begin{cases} 1/3 + 0.141x'_i - 0.12(x'_i)^2 + \\ \quad (1 + 0.5x'_i)(1 + x'_i)^{-2}, & x'_i \leq 0.5; \\ [\ln(1 + x'_i) + 0.06](x'_i)^{-1}, & 0.5 \leq x'_i \leq 3.5; \\ [\ln(1 + x'_i) + 0.5 - (2 + 0.076x'_i)^{-1}](x'_i)^{-1}, & 3.5 \leq x'_i. \end{cases}$$

To test if the scattering event will occur, we draw a random number  $\xi_s$ . If  $\xi_s < \sigma(x'_i)/\sigma_T$  is satisfied, the scattering event occurs.

If the scattering event is determined to occur, we perform an acceptance-rejection for the direction and energy of

the photon after the scattering event. We first draw 3 random numbers  $\xi_1, \xi_2, \xi_3$ . The random numbers  $\xi_1, \xi_2$  are used to compute the angles

$$\begin{aligned}\mu'_f &= \frac{\beta'_{e,i} + 2\xi_1 - 1}{1 + \beta'_{e,i}(2\xi_1 - 1)} \\ \phi'_f &= 2\pi\xi_2.\end{aligned}$$

From  $\mu'_f, \phi'_f$ , we can compute the direction of the photon after the scattering event with the expressions

$$\begin{aligned}\Omega'_{1,f} &= \mu'_f v'_{3,i} + \sqrt{1 - (\mu'_f)^2} \rho^{-1} (v'_{2,i} \cos \phi'_f + v'_{1,i} v'_{3,i} \sin \phi'_f) \\ \Omega'_{2,f} &= \mu'_f v'_{2,i} + \sqrt{1 - (\mu'_f)^2} \rho^{-1} (-v'_{1,i} \cos \phi'_f + v'_{2,i} v'_{3,i} \sin \phi'_f) \\ \Omega'_{3,f} &= \mu'_f v'_{3,i} + \sqrt{1 - (\mu'_f)^2} \rho \sin \phi'_f,\end{aligned}$$

where  $\rho = \sqrt{(v'_{1,i})^2 + (v'_{2,i})^2}$ . The next step is to compute the ratio of the dimensionless photon energy in the electron rest frame after scattering ( $x'_f$ ), to  $x'_i$ , with the equation

$$\frac{x'_f}{x'_i} = \left[ 1 + \frac{E'_{\gamma,i}(1 - \mathbf{\Omega}'_i \cdot \mathbf{\Omega}'_f)}{\gamma'_{e,i} m_e c^2 (1 - \mu'_f \beta'_{e,i})} \right]^{-1},$$

where  $\mathbf{\Omega}'_i \cdot \mathbf{\Omega}'_f = \Omega'_{1,i} \Omega'_{1,f} + \Omega'_{2,i} \Omega'_{2,f} + \Omega'_{3,i} \Omega'_{3,f}$  is the angle between the initial photon direction and the final photon direction. To determine if the final photon energy and direction is accepted, we use  $\xi_3$  to test the acceptance-rejection condition

$$\begin{aligned}2\xi_3 &< \left( \frac{x'_f}{x'_i} \right)^2 \mathcal{X}, \text{ where} \\ \mathcal{X} &= \left( \frac{x'_f}{x'_i} \right)^{-1} + \frac{x'_f}{x'_i} + \frac{4}{x'_i} \left[ 1 - \left( \frac{x'_f}{x'_i} \right)^{-1} \right] + \frac{4}{(x'_i)^2} \left[ 1 - \left( \frac{x'_f}{x'_i} \right)^{-1} \right]^2.\end{aligned}$$

If the condition  $2\xi_3 < (x'_f/x'_i)^2 \mathcal{X}$  is satisfied, the final photon direction is accepted and the energy of the photon after scattering is found with the expression  $E'_{\gamma,f} = (x'_f/x'_i) x'_i m_e c^2 [2\gamma'_{e,i} (1 - \mu'_f \beta'_{e,i})]^{-1}$ . Otherwise, we continue to draw 3 new random numbers  $\xi_1, \xi_2, \xi_3$  until the condition  $2\xi_1 < (x'_f/x'_i)^2 \mathcal{X}$  is satisfied.

## APPENDIX E: UPDATING ELECTRON ENERGY AND DIRECTION AFTER SCATTERING

In addition to updating the energy and direction of the photon after the scattering event, we also update the energy and direction of the electron. The energy of a photon-electron system is given by  $E' = E'_\gamma + m_e c^2 \gamma'_e$ . Using conservation of energy, we can find  $\gamma'_{e,f}$  with the expression

$$\gamma'_{e,f} = \frac{E'_{\gamma,i} - E'_{\gamma,f} + m_e c^2 \gamma'_{e,i}}{m_e c^2}.$$

The momentum of a photon-electron system is given by  $\mathbf{p}' = [(E'_\gamma/c)\mathbf{\Omega}'_1 + \|\mathbf{p}'_e\|v'_1]\hat{x} + [(E'_\gamma/c)\mathbf{\Omega}'_2 + \|\mathbf{p}'_e\|v'_2]\hat{y} + [(E'_\gamma/c)\mathbf{\Omega}'_3 + \|\mathbf{p}'_e\|v'_3]\hat{z}$ , where  $\|\mathbf{p}'_e\| = m_e c \beta'_e \gamma'_e$ . Using conservation of momentum in

each direction, we can find  $v'_{1,f}, v'_{2,f}, v'_{3,f}$  with the expressions

$$\begin{aligned}v'_{1,f} &= \frac{(E'_{\gamma,i}/c)\Omega'_{1,i} + m_e c \beta'_{e,i} \gamma'_{e,i} v'_{1,i} - (E'_{\gamma,f}/c)\Omega'_{1,f}}{m_e c \beta'_{e,f} \gamma'_{e,f}} \\ v'_{2,f} &= \frac{(E'_{\gamma,i}/c)\Omega'_{2,i} + m_e c \beta'_{e,i} \gamma'_{e,i} v'_{2,i} - (E'_{\gamma,f}/c)\Omega'_{2,f}}{m_e c \beta'_{e,f} \gamma'_{e,f}} \\ v'_{3,f} &= \frac{(E'_{\gamma,i}/c)\Omega'_{3,i} + m_e c \beta'_{e,i} \gamma'_{e,i} v'_{3,i} - (E'_{\gamma,f}/c)\Omega'_{3,f}}{m_e c \beta'_{e,f} \gamma'_{e,f}}.\end{aligned}$$

This paper has been typeset from a  $\text{\TeX}/\text{\LaTeX}$  file prepared by the author.